

Corso di Laurea Magistrale in Ingegneria Energetica e
Nucleare

Master thesis

**Neutron kinetics equations for
APOLLO3[®] code and application to
noise problems**



**POLITECNICO
DI TORINO**

Dipartimento
Energia

Thesis supervisors

Prof. S. Dulla
Prof. P. Ravetto

CEA tutor

Dr. S. Santandrea

Candidate

Andrea Gammicchia

July 2018

Abstract

A 2-D noise model is implemented in the deterministic reactor code APOLLO3[®] to simulate a periodic oscillation of a structural component. The Two/Three Dimensional Transport (TDT) solver, using the Method of Characteristics, is adopted for the calculation of the case studies, constituted by a detector and a control-rod assembly. The period is constructed by properly linking the geometries corresponding to the temporal positions. The calculation is entirely performed in the real time domain, without resorting to the traditional frequency approach. The periodicity allows to express the delayed fission source as a function of the flux values over time, instead of precursor concentrations. A dynamic eigenvalue is defined that takes into account the system average reactivity over a period. The algorithm is accelerated by combining the Wielandt shift scheme and the DP_N synthetic method. For each cell of the domain, the time values of fission rates are analysed to determine the noise extent: for this purpose maximum variations relative to the mean value over the period are plotted.

Acknowledgements

This work has been produced during six months spent at CEA centre of Saclay. Before leaving for Paris, I had not had a work/study experience abroad, nor had I lived alone for a long period yet: for me it would have been a unique opportunity to make up for these shortcomings at once. Moreover, the prestige of the institution that would welcome me represented a further reason to go. These months gave me the opportunity to meet really brilliant people and to enrich my knowledge in the nuclear field; at the same time, they have further broadened my horizons and my desire to learn.

First of all, I want to thank my parents for their great support in all these years of study and for having always believed in my potential. I have to thank my supervisors, Prof. S. Dulla and Prof. P. Ravetto, for making this experience possible, and Politecnico di Torino for the education I received. A special thanks to Simone Santandrea, for his fundamental guidance and advice, as well as for the patience with which he would clarify my several doubts. Thanks to the SERMA people with whom I collaborated and who gave me valuable suggestions for my work, in particular Igor Zmijarevic. Thanks to all my new friends for the very good time I had in Paris. And finally, thanks to Valentina for the tenacity and the love with which she remained at my side despite the distance.

Contents

1	Introduction	7
1.1	Neutron noise	7
1.2	Brief history	8
1.3	Methodologies	8
1.4	Goal definition and structure	9
2	Theoretical background	11
2.1	APOLLO3 [®] code system	12
2.2	Multi-group approximation	13
2.3	Introduction to self-shielding in APOLLO3 [®]	15
2.3.1	Sub-group method	16
2.3.2	Tone and Livolant-Jeanpierre methods	17
2.4	Iterative procedure for the solution of NTE	18
2.5	Method Of Characteristics	19
3	Model and equations	23
3.1	Frequency model	24
3.2	Our temporal model	27
3.2.1	Delayed-term treatment	29
3.2.2	Quadrature formula for the delayed source	30
3.2.3	Adiabatic approximation	32
3.2.4	Eigenvalue update	33
3.3	Description of studied systems	33
3.3.1	Case 1: detector	36
3.3.2	Case 2: control-rod assembly	37
3.4	A model for neutron leakage	40
4	Acceleration method	43
4.1	Wielandt scheme for outer iterations	43
4.2	DP_N synthetic acceleration	44
4.3	Performance comparison	46

5	Results	49
5.1	Fission-rate analysis	52
5.1.1	Detector	53
5.1.2	Control-rod assembly	55
6	Conclusions	59
A	Complex and real spherical harmonics	61

Chapter 1

Introduction

The present thesis deals with the neutron noise field and illustrates a research to develop better methods to simulate the phenomenon and to perform the diagnosis of the noise signal. It is the result of a six-month internship work, which took place between September 2017 and March 2018 at CEA¹ centre of Paris-Saclay.

This first chapter introduces some basic concepts regarding the topic, highlighting its strategic importance for nuclear industry, together with a historical recap from its “discovery”, in the first half of the last century, until nowadays. Moreover, the characteristics of traditional simulation methods are outlined, followed by an introduction to the new method implemented by this work. Lastly, the paper structure is described.

1.1 Neutron noise

In physics a noise represents a disturbance, a small and generally periodic deviation of the quantities from the stationary values. It follows that noise can occur and potentially be detected only in real systems being monitored over time. Dealing with neutronics the system is of course the reactor core, with the ensemble of subsystems which compose it, and the noise affects the neutron flux as a result of perturbations of macroscopic cross sections; these are due either to vibrations of the structural components or to fluctuations of the coolant density. This is usually referred to as “power reactor noise”, as opposed to the “zero power reactor noise” typical of multiplying systems where material properties are constant.² In the present thesis only the former is considered. Whenever the excursions exceed the safety limits, noise signal can be analysed to identify and localize malfunctions without the need of destructive diagnostics. In this sense the improvement in the capability of our instruments of detecting the neutron noise signal and the development of more sophisticated and efficient methods to elaborate it go hand

¹Commissariat à l'Énergie Atomique et aux Énergies Alternatives.

²In zero power noise the analysed fluctuation comes from the statistical nature of the neutron collision with matter. It is only important for low-power systems, where the neutron population is scarce. In this framework the variance of the neutron flux is comparable to its mean value and is therefore detectable.

in hand with higher levels of safety, which is notoriously of fundamental importance in the nuclear field.

1.2 Brief history

Neutron noise theory has its origins in the experiments performed at the "Clinton Pile" of Oak Ridge in 1940s [10], whose goal was the evaluation of absorption cross sections of various elements. Although they did not concern diagnostics at all, these experiments contemplated, for the first time, neutron oscillations. The analyses of these measurements were collected in a paper by Weinberg and Schweinler in 1948 [22].

Noise diagnostics in neutronics was born several years later when, again in Oak Ridge, measurements performed in the High Flux Isotope Reactor showed how a peak in the frequency spectrum, given by neutron detectors, could be traced back to an anomalous control-rod vibration (the experience was described by Fry in 1971 [5]). This was followed by several studies and analyses on real power plants during the 1970s, and by eight symposia on the topic (known as SMORN, Specialist Meetings On Reactor Noise).

After this golden period, the interest in neutron noise gradually diminished: in fact, during the 1990s and until the mid-2000s noise analysis was only carried out by universities rather than, as previously, by big research centres and industries [13].

More recently, new developments have been encouraged by the search for higher levels of safety, but above all by German nuclear industry: E.ON had problems with anomalous vibrations on some of its Pre-Konvoi reactors installed in Germany and Spain, for which it was forced to lower their nominal power, and therefore decided to invest in improving noise methods for diagnostics.

1.3 Methodologies

Traditionally, neutron noise can be simulated by a stochastic model generating the small deviations randomly or by considering a fixed, periodic modification of the cross sections [16]. In both cases the common starting point is a critical condition and the change of cross sections, acting as noise source, produces fluctuations in the neutron flux which can be either random or deterministic, depending on the nature of the source [10].

These oscillations are usually analysed by means of a frequency-based approach: as will be shown later and is described in [10, 13], this method considers a perturbed equation, derived from Boltzmann's, which is Fourier transformed in order to obtain linearized equations in the frequency domain. A drawback of this procedure is the appearance of a frequency dependence in cross sections, with consequent complications in the numerical discretizations.

The possibility of avoiding such a problem, alongside with the absence of complex values to deal with are the principal advantages of our method.

1.4 Goal definition and structure

This thesis aims to illustrate an alternative deterministic approach for the analysis of noise problems: once the noise source has been chosen among different possible oscillating elements (a control assembly, a detector), the dynamic behaviour of the system is described by means of different geometric configurations which follow each other to simulate its evolution along a period of oscillation. In so doing, the goal is to point out what results from this induced noise: the fission-rate fluctuations in the different regions are chosen for this purpose as monitored quantities. The distribution of their oscillation amplitudes is therefore obtained in the whole domain.

This work is implemented in CEA deterministic code APOLLO3[®] and exploits the potentiality of its version of the Two/Three Dimensional Transport (TDT) solver.

The paper is organized as follows:

chapter 2 The theory and the methods that form the basis of our work and in general of any deterministic approach to the solution of neutron Boltzmann equation are introduced;

chapter 3 Our noise model is described, illustrating our hypotheses and equations, together with the geometries considered. The traditional frequency model is also treated, showing its intrinsic difficulties. Lastly, space is given to the description of the leakage model adopted;

chapter 4 This chapter is dedicated to the acceleration method employed, which combines an original Wielandt scheme with a classic DP_N synthetic acceleration. Its performances are shown for a simple noise case;

chapter 5 Our results are shown, with regards to the eigenvalue obtained in the dynamic simulations and, in particular, to the amplitude of variation of the fission rates.

Chapter 2

Theoretical background

In the nuclear field all numerical methods aim to solve Boltzmann transport equation, whose time-dependent form for neutrons is here reported (its derivation is found in [3]):

$$\begin{aligned} \left(\frac{1}{v(E)} \partial_t + \vec{\Omega} \cdot \nabla + \Sigma_t(\vec{r}, E, t) \right) \psi(\vec{r}, \vec{\Omega}, E, t) = & q(\vec{r}, \vec{\Omega}, E, t) + \\ & \int_E dE' \int_{S_{\vec{\Omega}}} d\Omega' \Sigma_s(\vec{r}, \vec{\Omega}' \cdot \vec{\Omega}, E' \rightarrow E, t) \psi(\vec{r}, \vec{\Omega}', E', t) + \\ & \sum_{j=1, N_{isotopes}} \frac{\chi_j(E)}{4\pi} \int_E dE' \nu \Sigma_{f,j}(\vec{r}, E', t) \phi(\vec{r}, E', t). \end{aligned} \quad (2.1)$$

This integro-differential equation describes the behaviour of the neutron angular flux ψ in the $(\vec{r}, \vec{\Omega}, E)$ phase space over time. Due to the very high number of particles, neutron population is treated as a continuous fluid whose average properties are investigated in the neighbourhood of the phase space. The different terms are explained in the following:

$\vec{\Omega} \cdot \nabla \psi(\vec{r}, \vec{\Omega}, E, t)$: the streaming term, representing the net balance in the phase space between outgoing and incoming neutrons;

$\Sigma_t(\vec{r}, E, t) \psi(\vec{r}, \vec{\Omega}, E, t)$: the removal term due to interactions of neutrons (absorption and scattering);

$q(\vec{r}, \vec{\Omega}, E, t)$: the external source, usually negligible unless the system is source-driven sub-critical; this hypothesis is also valid during the start-up phase of power nuclear reactors;

$\int_E dE' \int_{S_{\vec{\Omega}}} d\Omega' \Sigma_s(\vec{r}, \vec{\Omega}' \cdot \vec{\Omega}, E' \rightarrow E, t) \psi(\vec{r}, \vec{\Omega}', E', t)$: the transfer term, given by neutrons emerging from scattering in $d\vec{r}$ around \vec{r} and acquiring direction $\vec{\Omega}$ and energy E ; $\int_E dE'$ and $\int_{S_{\vec{\Omega}}} d\Omega'$ stand for the integration over the whole energy domain and for the angular integral over the unit sphere, respectively;

$\sum_{j=1}^{N_{isotopes}} \frac{\chi_j(E)}{4\pi} \int_E dE' \nu \Sigma_{f,j}(\vec{r}, E', t) \phi(\vec{r}, E', t)$: the fission term, made by the contribution of each fissile isotope j to the number of neutrons emitted in the phase space by

fission, assuming the isotropy of the phenomenon; ϕ is the scalar flux equal to $\int_{S_{\vec{\Omega}}} d\Omega \psi(\vec{r}, \vec{\Omega}, E, t)$.

It is common practice to write (2.1) in a more compact form, which is obtained defining the transport term $\mathcal{L}\psi(\vec{r}, \vec{\Omega}, E, t)$ as the sum of the streaming and removal terms, and calling $\mathcal{H}\psi(\vec{r}, \vec{\Omega}, E, t)$ and $\mathcal{F}\phi(\vec{r}, E, t)$ the transfer and the fission terms, respectively. In this way, the initial equation becomes:

$$\left(\frac{1}{v}\partial_t + \mathcal{L} - \mathcal{H}\right)\psi(\vec{r}, \vec{\Omega}, E, t) = \mathcal{F}\phi(\vec{r}, E, t). \quad (2.2)$$

In order to well pose this problem, boundary and initial conditions are required:

$$\psi(\vec{r}_s, \vec{\Omega}_{in}, E, t) = \psi_{in}(E, t) \quad \vec{r}_s \in \partial D, \quad \hat{n} \cdot \vec{\Omega}_{in} < 0, \quad (2.3)$$

\hat{n} being the versor normal to the contour of the domain ∂D ,

$$\psi(\vec{r}, \vec{\Omega}, E, t = 0) = \psi_0(\vec{r}, \vec{\Omega}, E). \quad (2.4)$$

An analytical solution for (2.1) is not available for general cases: one-dimensional cases can be solved analytically only under certain assumptions regarding the medium, the energy range and the spatial and temporal dependence of the source, whereas 2-D and 3-D problems almost always require a numerical solution, unless the medium is void or purely absorbing [4].

To solve Boltzmann equation, nuclear industries can rely on two categories of computational methods: the stochastic and the deterministic ones. The former require the use of Monte-Carlo methods and simulate what occurs in reality by following each neutron, from the moment it is generated to its absorption; all possible interactions are considered in this process: fission, capture, scattering, (n,2n) reactions, etc. In this way, the macroscopic behaviour of the system is reconstructed analyzing what happens on a microscopic scale. On the other hand, deterministic methods aim to obtain a numerical solution of the transport equation through approximations that make the starting problem solvable by computer schemes. This is achieved by discretizing the domains of the variables involved, and of course the more accurate the discretization, the greater the accuracy of the solution. The advantage of these latter methods lies precisely in the possibility of obtaining a rather accurate solution in a relatively short time (with respect to stochastic methods).

Since, as already mentioned, the present work is produced using the Two/Three Dimensional Transport (TDT) solver of APOLLO3[®] code, our discussion will now focus on an introduction to this deterministic tool, based on [4].

2.1 APOLLO3[®] code system

APOLLO3[®] was started by CEA in 2012 [19], after almost thirty years of use of its predecessor APOLLO2. Like any other deterministic code, at the moment, it

faces the reactor calculation in two steps: firstly, a detailed calculation of Boltzmann equation is performed on a small domain, which should be as indicative as possible of the global system (a fuel cell, an assembly or a cluster of assemblies), considering an infinite system obtained by reflective/translational/rotational conditions. This first step, called “lattice” calculation, requires very fine meshes in energy and space to obtain, by equivalence methods preserving lattice reaction rates, homogenized in space and condensed in energy cross sections to be used successively. The second step is the “core” calculation, performing a 3-D calculation on the whole domain with the real boundary conditions, but using a degraded solver.

In passing from the first phase to the second cross-section condensation is a very delicate operation: due to resonances, it may be quite tricky to guarantee the conservation of reaction rates: self-shielding formalism deals with this problem.

As it will be explained in chapter 3, we will limit our attention to the first phase, merely carrying out the self-shielding and the transport calculation on a 2-D system. To understand our procedure, in the following we will describe what gives rise to the need of performing the self-shielding, that is the multi-group approximation. The self-shielding formalism itself is then introduced.

2.2 Multi-group approximation

Nuclear deterministic methods subdivide the energy domain in a certain number N_g of discrete groups (281 in our case) and then consider just average distributions of neutrons inside each group. The following description is based on [4, 20].

To begin with, consider the steady-state form of the transport equation:

$$\begin{aligned} & [\vec{\Omega} \cdot \nabla + \Sigma_t(\vec{r}, E)]\psi(\vec{r}, \vec{\Omega}, E) = \\ & \int_E dE' \int_{S_{\vec{\Omega}}} d\Omega' \Sigma_s(\vec{r}, \vec{\Omega}' \cdot \vec{\Omega}, E' \rightarrow E)\psi(\vec{r}, \vec{\Omega}', E') + \\ & \frac{1}{k_{eff}} \sum_{j=1}^{N_{iso}} \frac{\chi_j(E)}{4\pi} \int_E dE' \nu \Sigma_{f,j}(\vec{r}, E')\phi(\vec{r}, E'), \end{aligned} \quad (2.5)$$

where k_{eff} is the effective multiplication factor, necessary to guarantee stationarity. Referring to (2.5), it can be expressed as

$$k_{eff} = \frac{4\pi \int_D d\vec{r} \int_E dE \mathcal{F}\phi(\vec{r}, E)}{\int_D d\vec{r} \int_E dE \int_{S_{\vec{\Omega}}} d\Omega (\mathcal{L} - \mathcal{H})\psi(\vec{r}, \vec{\Omega}, E)} \quad (2.6)$$

that is, as the ratio between the total number of neutrons produced and removed in all the phase spaces. Depending on its value, a system is defined as sub-critical ($k_{eff} < 1$), critical ($k_{eff} = 1$) or super-critical ($k_{eff} > 1$).

Now, identifying the multi-group angular flux as

$$\psi^g(\vec{r}, \vec{\Omega}) = \int_g dE \psi(\vec{r}, \vec{\Omega}, E) \quad (2.7)$$

and analogously the multi-group scalar flux $\phi^g(\vec{r})$, one can write eq. (2.5) in terms of ψ^g and ϕ^g by simply integrating the equation over an energy group. This yields the multi-group steady-state transport equation

$$\begin{aligned} & [\vec{\Omega} \cdot \nabla + \Sigma_t^g(\vec{r}, \vec{\Omega})] \psi^g(\vec{r}, \vec{\Omega}) = \\ & \sum_{g'=1}^{N_g} \int_{S_{\vec{\Omega}}} d\Omega' \Sigma_s^{g'g}(\vec{r}, \vec{\Omega}', \vec{\Omega}) \psi^{g'}(\vec{r}, \vec{\Omega}') + \\ & \frac{1}{k_{eff}} \sum_{j=1}^{N_{iso}} \frac{\chi_j^g}{4\pi} \sum_{g'=1}^{N_g} \nu \Sigma_{f,j}^{g'}(\vec{r}, \vec{\Omega}) \phi^{g'}(\vec{r}), \end{aligned} \quad (2.8)$$

where the multi-group condensed cross sections Σ_t^g , $\Sigma_s^{g'g}$, $\Sigma_{f,j}^{g'}$ are defined so as to preserve the reaction rates over the energy group. For instance, considering just the total cross section, its condensed version is given by

$$\Sigma_t^g(\vec{r}, \vec{\Omega}) = \frac{\int_g dE \Sigma_t(\vec{r}, E) \psi(\vec{r}, \vec{\Omega}, E)}{\int_g dE \psi(\vec{r}, \vec{\Omega}, E)}. \quad (2.9)$$

It is common practice to neglect the angular dependence in (2.9) in order to avoid excessive memory storage (this is done by simply weighting the cross sections with the scalar flux). Moreover, it is apparent that condensation requires the knowledge of the flux, which is precisely our unknown. Therefore, an approximated value for $\phi(\vec{r}, E)$ must be used and, as will be clarified below, the quality of this approximation has a strong impact on the validity of condensed values.

An intuitive way to satisfy (2.9) for any kind of interactions, neglecting the dependence on direction, is to evaluate the condensed cross sections of reaction ρ for any isotope j as

$$\sigma_{\rho,j}^g(\vec{r}) = \frac{\int_g dE \sigma_{\rho,j}(E) \phi(\vec{r}, E)}{\int_g dE \phi(\vec{r}, E)}. \quad (2.10)$$

For non-resonant isotopes or outside the resonance range (from some eV to some hundreds of keV, depending on the isotope), microscopic cross sections vary slowly as a function of energy. Therefore, the weighting function can be approximated by a space-independent energy spectrum $\phi_w(E)$, representative of the system considered. This leads to the definition of so-called “infinite-dilution” multi-group cross sections, which can be computed once and for all for the neutron spectrum of interest. However, if the same approach is adopted for the resonance domain, that is, if a slowing-down spectrum is considered regardless of the spatial position, completely wrong results are produced, since reaction rates would be overestimated and the resulting k_{eff} could be several tens of percent lower than the real one. Hence, a correct procedure cannot ignore the real geometry of the problem, because the errors made in localized regions (for instance, in the outermost layer of the fuel, where the flux is relatively high but there are many resonant isotopes) may compromise the final result.

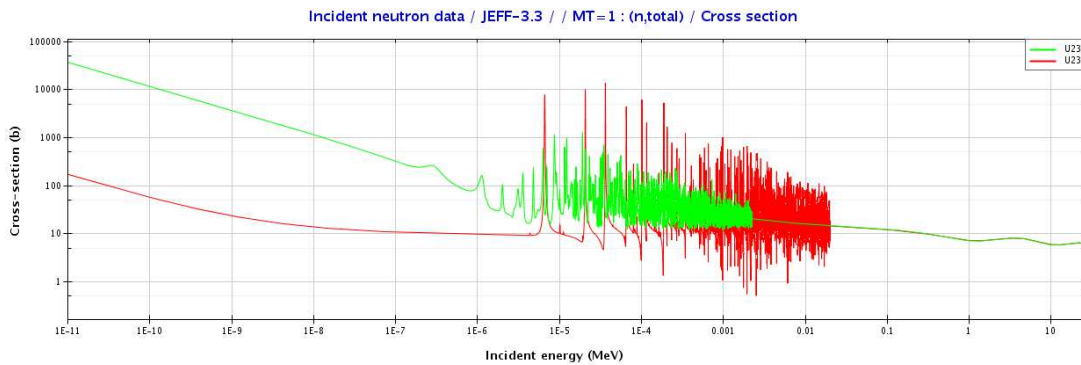


Figure 2.1: Total microscopic cross sections of uranium 235 and 238 as a function of energy [9]. Resonances clearly characterize the epithermal energy range.

Self-shielding methods have the delicate task of providing reasonably accurate model for the flux, which is needed in the resonance range to obtain energy-condensed values for the different homogenized regions the system is divided into.

2.3 Introduction to self-shielding in APOLLO3[®]

This paragraph is meant as a mere introduction to the topic, since an in-depth dissertation falls beyond the interest of this work. To go into more detail the reader may consult references [4, 7, 8, 18], from which the following introduction is taken.

By “self-shielding” one denotes the effect of a resonance on the reaction rate: in a very narrow energy range, the cross section (absorption, scattering or total one) may increase of several orders of magnitude (see Fig. 2.1), causing a localized tip for the flux, which is all the more pronounced the more the interaction probability increases. These two effects compensate each other and, as a consequence, the reaction rate variation is lower than the ones of the flux and of the cross section. Taking into account this phenomenon, occurring in regions where resonant isotopes are present and therefore depending on the real geometry of the system, leads to the evaluation of self-shielded multi-group cross sections.

Three major self-shielding techniques have been implemented in APOLLO3[®] : the sub-group method (SGM), Tone method and Livolant-Jeanpierre method. They all approximate the scalar in-group flux $\phi(\vec{r}, E)$, but adopting different strategies. Some hypotheses are in common, though: in the fissile mixture, for one isotope at a time a fine cross-section energy structure is considered, while group-averaged cross sections are used for the others, treated as moderators. An iterative procedure among isotopes is then required to obtain consistent multi-group values. This approach introduces errors which are reduced as long as the second common hypothesis is valid, that is the narrow-resonance approximation: according to it, resonances of different isotopes do not overlap (obviously, the finer the energy mesh and the more accurate this assumption becomes). This makes it also reasonable to treat transfer probabilities and emission

spectra as constant within each energy group, because, if the energy discretization is fine enough, transfer from other groups represents the major contribution of in-group emission. Moreover, all shielding methods of APOLLO3[®] assume that the scattering is isotropic and apply then the same shielding factor, valid for infinite-dilution values and therefore constant over an energy group, to obtain the anisotropic scattering cross sections.

Tone and Livolant-Jeanpierre methods are both based on an equivalence principle, allowing to retrieve self-shielded cross sections from pre-tabulated library functions of infinite-dilution cross sections, whereas the Sub-group method has a different approach, which is briefly described below. After that, the other two methods will be treated.

2.3.1 Sub-group method

The sub-group method evaluates the flux within group g for isotope j as solution of the slowing-down problem

$$\begin{aligned}
[\vec{\Omega} \cdot \nabla + \hat{\Sigma}_t(\vec{r}, E)]\psi(\vec{r}, \vec{\Omega}, E) = & \\
f_j(g \rightarrow g)N_j(\vec{r}) \int_g dE \sigma_{s,j}(E)\phi(\vec{r}, E) + & \\
\sum_{k \neq j} f_k(g \rightarrow g)N_k(\vec{r})\sigma_{s,k}^g(\vec{r})\phi^g(\vec{r}) + & \\
\sum_{k, g' \neq g} f_k(g' \rightarrow g)N_k(\vec{r})\sigma_{s,k}^{g'}(\vec{r})\phi^{g'}(\vec{r}) + & \\
\frac{1}{k_{eff}} \sum_{k, g'} \frac{\chi_k^g}{4\pi} N_k(\vec{r})\nu\sigma_{f,k}^{g'}(\vec{r})\phi^{g'}(\vec{r}), & \quad (2.11)
\end{aligned}$$

where isotopic transfer probabilities f_k and per-group emission spectra χ_k^g are known values that can be found in nuclear libraries, N represents the isotope density (expressed in $[cm^{-3}]$) and $\hat{\Sigma}_t$ is the sum of the contributions of the isotope being considered (j) and of background isotopes (k):

$$\hat{\Sigma}_t(\vec{r}, E) = N_j(\vec{r})\sigma_{t,j}^g(E) + \sum_{k \neq j} N_k(\vec{r})\sigma_{t,k}^g(\vec{r}). \quad (2.12)$$

In (2.11), the transfer term is divided into three parts:

$f_j(g \rightarrow g)N_j(\vec{r}) \int_g dE \sigma_{s,j}(E)\phi(\vec{r}, E)$: in-group scattering due to isotope j ;

$\sum_{k \neq j} f_k(g \rightarrow g)N_k(\vec{r})\sigma_{s,k}^g(\vec{r})\phi^g(\vec{r})$: in-group scattering due to background isotopes;

$\sum_{k, g' \neq g} f_k(g' \rightarrow g)N_k(\vec{r})\sigma_{s,k}^{g'}(\vec{r})\phi^{g'}(\vec{r})$: scattering from other groups.

As already said, only the first term maintains a fine energy dependence. Denoting by $q^g(\vec{r})$ the right-hand side of (2.11), and by $\mathcal{K}(\vec{r}, E)$ the inverse transport operator integrated

over directions, one obtains an equation for the in-group scalar flux to be used in (2.10):

$$\phi(\vec{r}, E) = \mathcal{K}(\vec{r}, E)q^g(\vec{r}). \quad (2.13)$$

Its solution requires the convergence of an iteration process over all groups, and for each group an iteration over isotopes is needed, updating their multi-group cross sections with the values of the already computed isotopes. This evaluation is made by means of probability tables [12], providing weights to estimate integrals over energy groups through quadrature formulas. Lastly, homogenized values relative to self-shielding regions are obtained by approximating the operator \mathcal{K} using the collision probability method (CPM, a description can be found in [4]).

2.3.2 Tone and Livolant-Jeanpierre methods

These methods are based on an equivalence between the real heterogeneous medium and an infinite homogeneous one. According to Tone, for each self-shielding region i and isotope j the flux is computed as

$$\phi_i(E) = \frac{D}{\sigma_{t,j}(E) + \sigma_{0,j,i}^g}, \quad (2.14)$$

where D is a constant, $\sigma_{t,j}(E)$ the microscopic total cross section of isotope j and $\sigma_{0,j,i}^g$ represents the background cross section, given by the contributions of all the other isotopes in all regions x . Considering the collision probability $P_{ix}(E)$, which expresses as a function of energy the probability for a neutron born in region x to undergo its first collision in region i , Tone approximation states that its energy dependence is only given by the region of collision i ($P_{ix}(E) = f_i^g(E)P_{ix}^g$). This makes it possible to obtain, using CPM, the background cross section as

$$\sigma_{0,j,i}^g = \frac{\sum_x P_{ix}^g \sum_{k \neq j} N_{k,i} \sigma_{t,k,x}^g}{\sum_x P_{ix}^g N_{k,x}}, \quad (2.15)$$

Eq. (2.14) has the same shape of the relation for the flux valid for an infinite homogeneous medium: in fact, each region of the system can be seen as an infinite and homogeneous domain with a characterizing background cross section $\sigma_{0,j,i}^g$. Self-shielded cross sections are then computed using probability tables as in SGM, but adopting (2.14) as weighting spectrum for quadrature formulas.

Livolant-Jeanpierre strategy differs from Tone's for the equivalence procedure followed. As described in [7], by considering a system composed of N zones containing fuel and L with moderators, if each zone contains only one isotope the fundamental equation for each fuel zone i reads

$$V_i \Sigma_{o,i} \varphi_{o,i} = \sum_{x=1,N} V_x P_{ix} \mathcal{R}_o \varphi_{o,x} + \sum_{x=1,L} V_x P_{ix} \Sigma_x, \quad (2.16)$$

where o is the subscript for the fuel, V denotes the zone volume, Σ the total cross section, φ the fine-structure flux and \mathcal{R} the slowing-down operator, such that $\mathcal{R}_o \varphi_{o,x} =$

$\int_{u-\epsilon_x}^u du' \Sigma_{s,x}(u' \rightarrow u) \varphi_{o,x}$, ϵ_x being the maximum gain in lethargy u . Eq. (2.16) is clearly a heterogeneous problem with source. By exploiting the reciprocity property of collision probabilities ($V_x P_{ix} \Sigma_{o,x} = V_i P_{xi} \Sigma_{o,i}$) and since, under the hypothesis of narrow resonances, $\frac{\mathcal{R}_o \varphi_{o,x}}{\Sigma_{o,x}} = \frac{\mathcal{R}_o \varphi_{o,i}}{\Sigma_{o,i}}$, the previous equation becomes

$$\mathcal{R}_o \varphi_{o,i} - (\Sigma_{o,i} + \Sigma_{e,i}) \varphi_{o,i} + \Sigma_{e,i} = 0, \quad (2.17)$$

where the equivalent cross section $\Sigma_{e,i}$ is defined as $\Sigma_{e,i} = \Sigma_{o,i} \frac{1 - \sum_{x=1,N} P_{xi}}{\sum_{x=1,N} P_{xi}}$. Eq. (2.17) represents the homogeneous problem equivalent, by means of $\Sigma_{e,i}$, to the original one; its solution $\varphi_{o,i}$ is used to compute multi-group shielded cross sections.

In our case Livolant-Jeanpierre method is adopted, alongside with a multi-cell approximation (MCA, its description can be found in [8]), which speeds up CP calculations.

2.4 Iterative procedure for the solution of NTE

The solution of the multi-group problem (2.8) is obtained by a three-level iterative scheme, in which three types of iterations are used: outer, thermal and inner, the second and the third being nested in the previous one. What follows is based on [20].

The outer iterations (index o) are solved according to the power method: by compacting (2.8) as

$$(\mathcal{L} - \mathcal{H}) \psi_{o+1}^g(\vec{r}, \vec{\Omega}) = \frac{1}{k_{eff,o}} \mathcal{F} \phi_o^g(\vec{r}), \quad (2.18)$$

one obtains the iterative form of the equation to be solved for each energy group, starting from initial guesses of ϕ_o^g and $k_{eff,o}$.

The thermal iterations (index t) cycle over groups maintaining the fission source constant, until the multi-group angular flux $\psi^g(\vec{r}, \vec{\Omega})$ has reached convergence in all of them. Groups are considered from the highest energy to the lowest, and for each one an inner iteration (index i) is performed, solving the problem

$$\mathcal{L} \psi_{i+1}^g(\vec{r}, \vec{\Omega}) = \int_{S_{\vec{\Omega}}} d\Omega' \Sigma_s^{gg}(\vec{r}, \vec{\Omega}' \cdot \vec{\Omega}) \psi_i^g(\vec{r}, \vec{\Omega}') + S^g(\vec{r}, \vec{\Omega}), \quad (2.19)$$

where S^g is made by the sum of the fission source, relative to the outer step “ o ”, and the contributions to the scattering from higher ($g' < g$, thermal step “ $t+1$ ”) and lower ($g' > g$, thermal step “ t ”) energy groups:

$$\begin{aligned} S^g(\vec{r}, \vec{\Omega}) &= \frac{1}{k_{eff,o}} \sum_{j=1}^{N_{iso}} \frac{\chi_j^g}{4\pi} \sum_{g'=1}^{N_g} \nu \Sigma_{f,j}^{g'}(\vec{r}, \vec{\Omega}) \phi_o^g(\vec{r}) + \\ &+ \sum_{g' < g} \int_{S_{\vec{\Omega}}} d\Omega' \Sigma_s^{g'g}(\vec{r}, \vec{\Omega}' \cdot \vec{\Omega}) \psi_{t+1}^{g'}(\vec{r}, \vec{\Omega}') + \\ &+ \sum_{g' > g} \int_{S_{\vec{\Omega}}} d\Omega' \Sigma_s^{g'g}(\vec{r}, \vec{\Omega}' \cdot \vec{\Omega}) \psi_t^{g'}(\vec{r}, \vec{\Omega}'). \end{aligned} \quad (2.20)$$

More details about this last iteration level will be provided in the next section.

At the end of each outer iteration, the fission term is updated with the new values ϕ_{o+1}^g of the multi-group scalar flux. Hence, the new $k_{eff,o+1}$ reads

$$k_{eff,o+1} = k_{eff,o} \frac{\sum_g \int_{\mathcal{D}} d\vec{r} \mathcal{F} \phi_{o+1}^g(\vec{r})}{\sum_g \int_{\mathcal{D}} d\vec{r} \mathcal{F} \phi_o^g(\vec{r})}. \quad (2.21)$$

The outer and the nested cycles are repeated until the convergence of k_{eff} .

2.5 Method Of Characteristics

To conclude the description of our theoretical framework we introduce here the Method Of Characteristics (MOC), which is employed in our calculation. This paragraph is taken from [4] and [20].

This method dates back to the studies carried out by Riemann in 1800s; more recently, its application in neutronics was proposed by J. R. Askew in 1972 [2]. One of its advantages is the capability to treat complex arbitrary geometries with a good compromise between precision and computational time.

As it is known, Boltzmann equation contains partial derivatives: the idea of MOC is to solve the problem along characteristic lines, for which it translates into an ordinary differential equation. Starting from (2.8) and considering the curve of points \vec{r} described by $\vec{r}(s) = \vec{r}_0 + s\vec{\Omega}$, with \vec{r}_0 constant and $\vec{r}_0 \perp \vec{\Omega}$, the $\vec{\Omega} \cdot \nabla \psi^g(\vec{r}, \vec{\Omega})$ term can be rewritten as

$$\vec{\Omega} \cdot \nabla \psi^g(\vec{r}, \vec{\Omega}) = \frac{d\psi^g(\vec{r}_0 + s\vec{\Omega}, \vec{\Omega})}{ds}, \quad (2.22)$$

where, since the characteristic direction $\vec{\Omega}$ is fixed, the right-hand side is now a total derivative. To exploit the potentiality of this approach, the entire domain D is subdivided in a set of homogeneous regions D_i , inside which the multi-group cross sections and the emission term $q^g(\vec{r}, \Omega)$ (given by the sum of scattering and fission term in the r.h.s. of (2.8)) are assumed as spatially constant. The continuous angular variable is discretized in a discrete set of directions, according to the classical S_N formalism (a possible reference is [3]): basically, we use a quadrature set $\{w_n, \vec{\Omega}_n, n = 1, N\}$ such that $\int_{S_{\vec{\Omega}}} d\Omega f(\vec{\Omega}) \approx \sum_{n=1, N} w_n f(\vec{\Omega}_n)$, where N is equal to the chosen number of directions and w_n the weight associated with the n^{th} direction. As shown in Fig. 2.2, for a chosen direction $\vec{\Omega}$, a bundle of characteristic lines parallel to it crosses the domain. Each region D_i can therefore be approximated as a set of rectangles having as dimensions the chords identified by the characteristics and the transversal step (equal to the distance between the lines). Clearly, the higher the number of characteristics and the closer this approximation will be to the real volume of the region.

Given these hypotheses, the solution of the multi-group transport equation relative

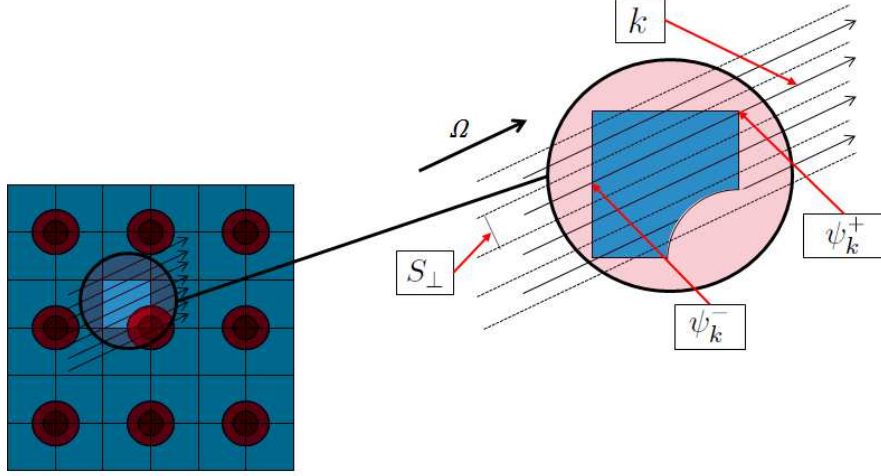


Figure 2.2: Characteristic lines crossing the domain. On the right a zoomed view on a single region is shown, pointing out for a generic line k its associated cross-sectional area S_{\perp} and the angular flux values at the entrance (ψ_k^-) and at the exit (ψ_k^+) of the region.

to the characteristic line k of direction $\vec{\Omega}$ inside D_i and for group g reads

$$\psi_k^g(s) = \psi_k^g(0) \exp(-\Sigma_{t,i}^g s) + q_i^g(\vec{\Omega}) \frac{1 - \exp(-\Sigma_{t,i}^g s)}{\Sigma_{t,i}^g}, \quad (2.23)$$

where $\psi_k^g(s)$ is considered as constant over the cross-sectional area S_{\perp} , perpendicular to line k . Evaluating (2.23) at the end of the chord, we obtain the transmission equation:

$$\psi_k^{g+} - \psi_k^{g-} = \left(\frac{q_i^g(\vec{\Omega})}{\Sigma_{t,i}^g} - \psi_k^{g-} \right) [1 - \exp(-\Sigma_{t,i}^g I_{k,i})], \quad (2.24)$$

where $I_{k,i}$ is the chord length and ψ_k^{g+} and ψ_k^{g-} correspond to the entrance ($-$) and the exit ($+$) of the region, that is, to the chord extremes.

In order to have information about $\bar{\psi}_i^g$, the average angular flux of group g in region i , and therefore to update the value of q_i^g according to the algorithm described in the previous section, a balance equation is required. This is obtained by averaging (2.8) on the region volume:

$$\frac{\vec{\Omega} \cdot \int_{D_i} d\vec{r} \nabla \psi^g(\vec{r}, \vec{\Omega})}{\int_{D_i} d\vec{r}} + \frac{\Sigma_{t,i}^g \int_{D_i} d\vec{r} \psi^g(\vec{r}, \vec{\Omega})}{\int_{D_i} d\vec{r}} = \frac{q_i^g(\vec{\Omega}) \int_{D_i} d\vec{r}}{\int_{D_i} d\vec{r}}. \quad (2.25)$$

This yields, by applying the divergence theorem,

$$\Sigma_{t,i}^g \bar{\psi}_i^g(\vec{\Omega}) = q_i^g(\vec{\Omega}) - \frac{1}{V_i} \int_{\partial D_i} d\vec{r}_s \vec{\Omega} \cdot \hat{n} \psi^g(\vec{r}_s, \vec{\Omega}), \quad (2.26)$$

where \vec{r}_s denotes the set of positions on the boundary of region i and V_i is the volume of the region. As it is shown in [20], thanks to the subdivision of the region described above, the surface integral becomes simply

$$\frac{1}{V_i} \int_{\partial D_i} d\vec{r}_s \vec{\Omega} \cdot \hat{n} \psi^g(\vec{r}_s, \vec{\Omega}) = \frac{z(\vec{\Omega})}{V_i} \sum_{\substack{k \parallel \vec{\Omega} \\ k \cap D_i}} [\psi_k^{g+} - \psi_k^{g-}] = \Delta J_i^g(\vec{\Omega}). \quad (2.27)$$

If the transversal step is fixed (as it usually is), the integration weight $z(\vec{\Omega})$ does not depend on the single characteristic line but only on $\vec{\Omega}$. Hence, the balance equation can be written as

$$\Sigma_{t,i}^g \bar{\psi}_i^g(\vec{\Omega}) = q_i^g(\vec{\Omega}) - \Delta J_i^g(\vec{\Omega}). \quad (2.28)$$

It has to be noted that, according to [18], the angular dependence of the emission term relative to group g and region i is treated by means of an expansion over real spherical harmonics (see appendix A):

$$q_i^g(\vec{\Omega}) = \vec{A}(\vec{\Omega}) \cdot \vec{q}_{g,i}, \quad (2.29)$$

$\vec{A}(\vec{\Omega})$ being the vector of all spherical harmonics functions, which, for an order of scattering anisotropy equal to K , is defined as $\vec{A}(\vec{\Omega}) = \{A_k^l(\vec{\Omega}), k = 0, K \wedge l = -k, k\}$. $\vec{q}_{g,i}$, given by

$$\vec{q}_{g,i} = \Sigma_{s,i}^{gg} \vec{\Phi}_{g,i} + S_{g,ext}, \quad S_{g,ext} = \sum_{g' \neq g} \Sigma_{s,i}^{g'g} \vec{\Phi}_{g',i} + \delta_{0k} \mathcal{F}_{g,i} \bar{\phi}_i^g, \quad (2.30)$$

is the vector of the $(K+1)^2$ angular moments taking into account, for each moment, the scattering contribution from the same group g and from the other groups separately and, only for the zero-order moment, the fission contribution (as expressed by the Kronecker delta δ_{0k}). Here $\Sigma_{s,i}^{gg}$ is the diagonal scattering operator applied to the flux moment vector $\vec{\Phi}_{g,i}$ which, using the S_N quadrature formula, can be written as

$$\vec{\Phi}_{g,i} = \int_{S_{\vec{\Omega}}} d\Omega \vec{A}(\vec{\Omega}) \bar{\psi}_i^g(\vec{\Omega}) \approx \sum_{n=1,N} w_n \vec{A}(\vec{\Omega}_n) \bar{\psi}_i^g(\vec{\Omega}_n). \quad (2.31)$$

At each inner iteration, until the flux convergence in group g , $\vec{q}_{g,i}$ is updated through (2.30), keeping $S_{g,ext}$ constant, and therefore used in (2.29) to have the new value of the emission term to be substituted in the balance equation (2.28). Then, computing the ΔJ_i^g term by means of the transmission equation (2.24), the balance equation yields the average per-region angular flux $\bar{\psi}_i^g$ needed to finally update the flux moments through (2.31).

Chapter 3

Model and equations

This chapter describes the model we used, alongside with the equations and the geometries considered to simulate the dynamic behaviour of neutron noise phenomena. Moreover, the reasons which led us to develop this model are clarified, by highlighting the difficulties rising from a traditional frequency-based approach.

To begin with, it is worthwhile to consider the nature of our problem: starting from a static situation, where quantities undergo negligible oscillations, noise introduces a temporal behaviour in the system which cannot be ignored. Therefore, we are interested in a kinetic system of equations including, beside the time-dependent Boltzmann equation (2.1), the equations for the concentrations of delayed-neutron precursors, whose role is explained briefly below. For each family i of delayed neutrons and fissile isotope j , the latter read

$$\partial_t C_i^j(\vec{r}, t) = -\lambda_i^j C_i^j(\vec{r}, t) + \int_E dE' \beta_i^j(E') \nu \Sigma_{f,j}(\vec{r}, E', t) \phi(\vec{r}, E', t), \quad (3.1)$$

where

$C_i^j(\vec{r}, t)$ is the concentration per unit volume at time t of precursors of the i^{th} family of delayed neutrons, generated by fission of the isotope j ;

λ_i^j is the decay constant of the precursors of the i^{th} family for the isotope j ;

$\beta_i^j(E)$ is the energy distribution of the fraction of delayed neutrons of the i^{th} family produced by the isotope j .

The form (3.1) is coherent to the nuclear data that can be found in cross-section libraries such as JEFF [9].

Time-dependent problems require eq. (3.1) to take into account the different time-scales involved [21]: as it is well-known, while most neutrons generated by fission are emitted instantaneously (and therefore are called “prompt”), a small fraction of them appears with a certain delay, that is, when their precursor isotope decays. It follows that the emission rate of the so-called “delayed” neutrons is ruled by the decay process of the precursors and that, as a consequence, their lifetime is much longer than the average one

Table 3.1: *Delayed-neutron lifetimes relative to the fission of uranium 235 for eight precursor families. Data are taken from [4].*

Precursor family	$\tau_i = \frac{1}{\lambda_i} [\text{s}]$
1	$8.021 \cdot 10^1$
2	$3.535 \cdot 10^1$
3	$2.352 \cdot 10^1$
4	7.516
5	3.419
6	1.500
7	$6.117 \cdot 10^{-1}$
8	$2.813 \cdot 10^{-1}$
Average value	$1.302 \cdot 10^1$

($10^{-6} \div 10^{-3} \text{s}$, according to [4]), going from a few tenths to some tens of seconds (the values for uranium 235 are shown in Tab. 3.1). To underline this aspect, for each fissile isotope j the fission operator of (2.1) can be decomposed as the sum of the prompt and delayed contributions:

$$\frac{\chi_j(E)}{4\pi} \int_E dE' \nu \Sigma_{f,j}(\vec{r}, E', t) \phi(\vec{r}, E', t) = \frac{\chi_j^P(E)}{4\pi} \int_E dE' \left(1 - \sum_i \beta_i^j(E') \right) \nu \Sigma_{f,j}(\vec{r}, E', t) \phi(\vec{r}, E', t) + \sum_i \frac{\chi_{i,j}^D(E)}{4\pi} \lambda_i^j C_i^j(\vec{r}, t), \quad (3.2)$$

where χ_j^P and $\chi_{i,j}^D$ are, respectively, the prompt-neutron energy spectrum relative to the isotope j and the energy spectrum of i^{th} family delayed neutrons produced by the isotope j . It is now apparent that the set of equations (3.1) constitutes a closed system with the transport equation, the flux being dependent on precursor concentrations and vice-versa.

The discussion focuses now on the description of the model which is commonly used in the context of neutron noise.

3.1 Frequency model

Traditionally, noise is treated within the framework of the perturbation theory of the steady-state situation. This is for example the approach followed in [13]. The starting point is a critical condition given by (2.5) with $k_{eff} = 1$, here reported in a compact form (for simplicity, the dependence on the phase space is omitted):

$$\left(\mathcal{L}_0 - \mathcal{H}_0 - \hat{\mathcal{F}}_0 \right) \psi_0 = \mathcal{T}_0 \psi_0 = 0, \quad (3.3)$$

where $\hat{\mathcal{F}}_0$ is the fission operator $\hat{\mathcal{F}}_* = \sum_{j=1}^{N_{\text{isotopes}}} \frac{\chi_j(E)}{4\pi} \int_E dE' \nu \Sigma_{f,j}(\vec{r}, E') \int_{S_{\vec{\Omega}}} d\Omega_*$ in the reference state. A perturbation of cross sections is therefore imposed and the following kinetic equation has to be considered:

$$\left[\frac{1}{v} \partial_t + \mathcal{T}(t) \right] \psi(t) = 0. \quad (3.4)$$

As a result of the perturbation, the kinetic operator \mathcal{T} can be written as

$$\mathcal{T}(t) = \mathcal{T}_0 + \delta\mathcal{T}(t) \quad (3.5)$$

and, under the hypothesis of being in stationary regime (after an initial transient due to the onset of the perturbation), also the flux reads

$$\psi(t) = \psi_0 + \delta\psi(t), \quad (3.6)$$

where $\delta\psi$ is precisely the noise. The notation used in (3.5) and (3.6) emphasizes the different orders of magnitude of the terms: in fact, this procedure assumes both $\delta\mathcal{T} = o(\mathcal{T}_0)$ and $\delta\psi = o(\psi_0)$ (“small-perturbation formulation”, see [16]); this hypothesis leads to neglect the second-order term given by the effect of the perturbed kinetic operator on the perturbed flux ($\delta\mathcal{T}\delta\psi$). By further assuming that the system criticality is preserved and substituting the relation for $\mathcal{T}(t)$ and $\psi(t)$ into (3.4), one obtains the linearized problem

$$\left(\frac{1}{v} \partial_t + \mathcal{T}_0 \right) \delta\psi(t) = -\delta\mathcal{T}(t)\psi_0, \quad (3.7)$$

which is then Fourier-transformed to obtain the neutron noise standard equation:

$$\mathcal{T}_{0,\omega} \delta\psi(\omega) = -\delta\mathcal{T}(\omega)\psi_0, \quad \forall \omega \in \mathbb{R}, \quad (3.8)$$

ω being the angular frequency, which substitutes time as variable in the Fourier space, and $\mathcal{T}_{0,\omega} = i_u \frac{\omega}{v} + \mathcal{L}_0 - \mathcal{H}_0 - \hat{\mathcal{F}}_{0,\omega}$ (i_u is the imaginary unit). It is worth noting that the dependence of $\mathcal{T}_{0,\omega}$ on the angular frequency is not only due to the transform of the derivative term, but also to the fission operator $\hat{\mathcal{F}}_{0,\omega}$. The latter in turn acquires this dependence through the precursor concentrations, which, as said above, have to be considered when kinetic behaviours are treated. This aspect is clarified below.

Eq. (3.8) has to be solved for a chosen set of harmonics $\{\omega_n, n = 1, N\}$ (the most important ones according to the perturbation imposed): the values of $\delta\psi(\omega_n)$ obtained are therefore needed to retrieve the flux solution in the temporal domain. However, the transition to Fourier domain is not exactly a smooth process: beside the need to deal with complex quantities and the already anticipated frequency-dependence of the kinetic operator, an even worse complication arises when perturbed cross sections are Fourier-transformed, since at that point they too depend on ω .

What has been said becomes apparent by considering the time-dependent multi-group equation (whose steady-state version is reported in section 2.2) after the Fourier

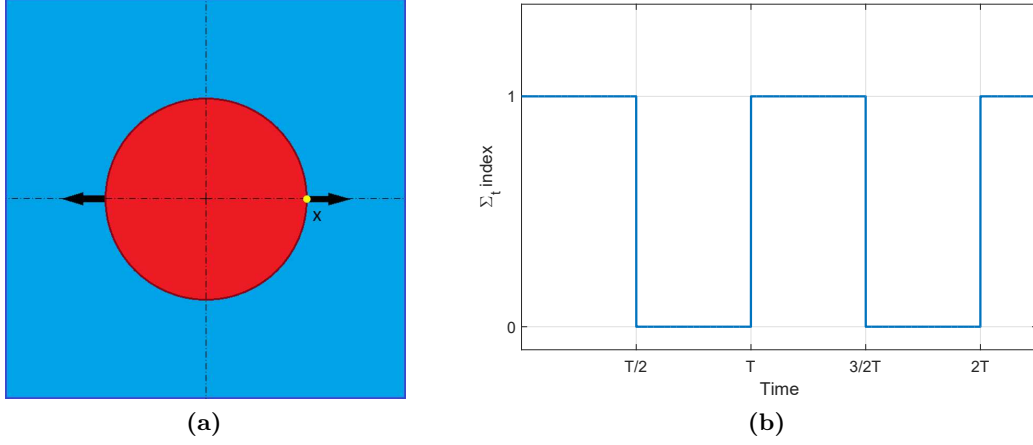


Figure 3.1: Example of a simplified fuel cell (a) with oscillating fuel rod. As shown in (b) for a T -periodic movement, the total cross section in point x assumes alternately the value of the fuel (index 1) and of the moderator (index 0).

transformation:

$$\begin{aligned}
& \left(i_u \frac{\omega}{\nu^g} + \vec{\Omega} \cdot \nabla + \Sigma_{t,0}^g(\vec{r}) \right) \delta\psi^g(\vec{r}, \vec{\Omega}, \omega) = \\
& \sum_{g'} \int_{S_{\vec{\Omega}}} d\Omega' \Sigma_{s,0}^{g'g}(\vec{r}, \vec{\Omega}' \cdot \vec{\Omega}) \delta\psi^{g'}(\vec{r}, \vec{\Omega}', \omega) + \\
& + \frac{1}{4\pi} \sum_j \left[\chi_j^{g,P} \sum_{g'} \left(1 - \sum_i \beta_i^{j,g'} \right) \nu \Sigma_{f,j,0}^{g'}(\vec{r}) \delta\phi^{g'}(\vec{r}, \omega) + \right. \\
& \left. + \sum_i \chi_{i,j}^{g,D} \frac{\lambda_i^j}{\lambda_i^j + i_u \omega} \sum_{g'} \beta_i^{j,g'} \nu \Sigma_{f,j,0}^{g'}(\vec{r}) \delta\phi^{g'}(\vec{r}, \omega) \right] + \\
& + q^g(\vec{r}, \vec{\Omega}, \omega). \tag{3.9}
\end{aligned}$$

q^g is the noise source ($-\delta\mathcal{T}\psi_0$ in (3.8)), given by

$$\begin{aligned}
q^g(\vec{r}, \vec{\Omega}, \omega) &= -\delta\Sigma_t^g(\vec{r}, \omega) \psi_0^g(\vec{r}, \vec{\Omega}) + \\
& + \sum_{g'} \int_{S_{\vec{\Omega}}} d\Omega' \delta\Sigma_s^{g'g}(\vec{r}, \vec{\Omega}' \cdot \vec{\Omega}, \omega) \psi_0^{g'}(\vec{r}, \vec{\Omega}') + \\
& + \frac{1}{4\pi} \sum_j \left[\chi_j^{g,P} \sum_{g'} \left(1 - \sum_i \beta_i^{j,g'} \right) \delta(\nu \Sigma_{f,j}^{g'}) (\vec{r}, \omega) \phi_0^{g'}(\vec{r}) + \right. \\
& \left. + \sum_i \chi_{i,j}^{g,D} \frac{\lambda_i^j}{\lambda_i^j + i_u \omega} \sum_{g'} \beta_i^{j,g'} \delta(\nu \Sigma_{f,j}^{g'}) (\vec{r}, \omega) \phi_0^{g'}(\vec{r}) \right]. \tag{3.10}
\end{aligned}$$

As discussed in section 2.3, the correct definition of multi-group cross sections requires the use of self-shielding techniques as a preliminary step before the iterative search for the solution. The expression of the noise source (3.10) shows that, following this kind of procedure, a further step is required: a priori, for each frequency considered a different spatial discretization has to be made, complicating the problem considerably. This may be clarified by the example in Fig. 3.1: consider a very simplified fuel cell, with the fuel rod oscillating horizontally along one of the axes with period T ; as a consequence, in the yellow x point of the axis the total cross-section value oscillates as well, as shown in the graph. Hence, the definition of $\delta\Sigma_t(t)$ in the frequency domain requires, for each spatial point, the calculation of Fourier transforms for all the N frequencies.

3.2 Our temporal model

The model developed in the present thesis is based on a quite different approach, aiming to avoid the difficulties caused by the passage to a complex domain. Instead of introducing the noise into the equations as a perturbation of the terms, our strategy consists in simulating a periodic oscillation geometrically: different states of the system are linked to represent its evolution during a period. A visual representation of this, together with the two case studies considered, is found in section 3.3. In this paragraph we deal with the description of the equations used and with the way the key quantities have been computed.

Our approach starts from the coupled kinetic system made by the precursor concentration equations (3.1) and the time-dependent transport equation (2.1), where the fission operator is expanded as in (3.2). As it is customary in literature ([10], for instance), we translate this system into one where precursors are only distinguished on a “family” base and not on their isotopic nature. To handle isotope-independent precursor concentrations we consider

$$C_i(\vec{r}, t) = \sum_j C_i^j(\vec{r}, t). \quad (3.11)$$

In order to apply the sum over fissile isotopes to all terms of (3.1) and to modify the delayed part of the fission operator, suitable definitions of the average per-family decay constants and delayed spectra are needed. The former can be written as

$$\bar{\lambda}_i(\vec{r}, t) = \frac{\sum_j \lambda_i^j C_i^j(\vec{r}, t)}{\sum_j C_i^j(\vec{r}, t)} \approx \lambda_i, \quad (3.12)$$

where the approximation is made that decay constants are only functions of the family of delayed neutrons, not of the isotope: the 8-group delayed family definition, used in this work, amply justifies this assumption [9]. Hence, from now on only λ_i will be used. The same simplification cannot be made for delayed spectra:

$$\bar{\chi}_i^D(\vec{r}, E, t) = \frac{\sum_j \chi_{i,j}^D(E) \lambda_i^j C_i^j(\vec{r}, t)}{\sum_j \lambda_i^j C_i^j(\vec{r}, t)} \approx \frac{\sum_j \chi_{i,j}^D(E) C_i^j(\vec{r}, t)}{\sum_j C_i^j(\vec{r}, t)}. \quad (3.13)$$

Although (3.13) exploits the approximation (3.12), $\bar{\chi}_i^D$ inherits a parasitic spatial and temporal dependence which cannot be neglected. Therefore, in the fission operator the delayed part now reads

$$\sum_j \sum_i \chi_{i,j}^D(E) \lambda_i^j C_i^j(\vec{r}, t) = \sum_i \bar{\chi}_i^D(\vec{r}, E, t) \lambda_i C_i(\vec{r}, t). \quad (3.14)$$

Using the formalism of nuclear data one can write delayed-neutron fractions as

$$\beta_i^j(E) = w_{d,i}^j P_{ed}^j(E), \quad (3.15)$$

separating the dependencies on energy and family with the use of the terms w_d and P_{ed} . Our system is then composed by the following equations:

$$\begin{aligned} & \left(\frac{1}{v} \partial_t + \vec{\Omega} \cdot \nabla + \Sigma_t(\vec{r}, E, t) \right) \psi(\vec{r}, \vec{\Omega}, E, t) = \\ & \int_E dE' \int_{S_{\vec{\Omega}}} d\Omega' \Sigma_s(\vec{r}, \vec{\Omega}' \cdot \vec{\Omega}, E' \rightarrow E, t) \psi(\vec{r}, \vec{\Omega}', E', t) + \\ & + \sum_j \frac{\chi_j^P(E)}{4\pi} \int_E dE' \left(1 - P_{ed}^j(E') \sum_i w_{d,i}^j \right) \nu \Sigma_{f,j}(\vec{r}, E', t) \phi(\vec{r}, E', t) + \\ & + \sum_i \frac{\bar{\chi}_i^D(\vec{r}, E, t)}{4\pi} \lambda_i C_i(\vec{r}, t), \end{aligned} \quad (3.16)$$

$$\begin{aligned} \partial_t C_i(\vec{r}, t) &= -\lambda_i C_i(\vec{r}, t) + \sum_j \int_E dE' w_{d,i}^j P_{ed}^j(E') \nu \Sigma_{f,j}(\vec{r}, E', t) \phi(\vec{r}, E', t), \\ & i = 1, 8. \end{aligned} \quad (3.17)$$

To construct the oscillation a set of static configurations is studied and their number has to match that of the time intervals in which the period is subdivided. However, not all kinetic parameters are recomputed for each state: we start considering the critical system not affected by the oscillation (for geometrical reasons, discussed in 3.3, we refer to it as “central static”). The self-shielding procedure treated in 2.3 is then performed only on this configuration, yielding the multi-group per-region cross sections to be used for the rest of the calculation. Moreover, the scalar flux ϕ^∞ , solution of the stationary equation

$$\begin{aligned} & \left(\vec{\Omega} \cdot \nabla + \Sigma_t(\vec{r}, E) \right) \psi^\infty(\vec{r}, \vec{\Omega}, E) = \\ & \int_E dE' \int_{S_{\vec{\Omega}}} d\Omega' \Sigma_s(\vec{r}, \vec{\Omega}' \cdot \vec{\Omega}, E' \rightarrow E) \psi^\infty(\vec{r}, \vec{\Omega}', E') + \\ & + \frac{\chi_j(E)}{4\pi} \int_E dE' \nu \Sigma_{f,j}(\vec{r}, E') \phi^\infty(\vec{r}, E') \end{aligned} \quad (3.18)$$

relative to the central static, is used to evaluate the delayed spectra to be adopted for all the static configurations, according to (3.13). For this scope stationary values of the

precursor concentrations $C_i^{j,\infty}$ are used, defined accordingly with the steady-state version of eq. (3.1):

$$C_i^{j,\infty}(\vec{r}) = \frac{\int_E dE' w_{d,i}^j P_{ed}^j(E') \nu \Sigma_{f,j}(\vec{r}, E') \phi^\infty(\vec{r}, E')}{\lambda_i}. \quad (3.19)$$

This strategy could be further improved by computing for each static case its own delayed spectra, but it is already more refined than common practice: usually, pre-tabulated spectra are used, result of weighting with model fluxes relative to infinite homogeneous media; on the contrary, our approach uses the real flux of the problem, although of the central static only.

It is good to specify that per-medium values are considered for the calculation: in fact, since different spatial regions may share the same medium¹, it is convenient to forget the region dependence by homogenizing over the medium volume. Therefore, per-medium and -family delayed spectra can be expressed as

$$\bar{\chi}_{i,M}^D(E) = \frac{\int_{V_M} d\vec{r} \bar{\chi}_i^D(\vec{r}, E)}{V_M}, \quad (3.20)$$

M being the medium index and V_M the medium volume, made by the volumes of all the regions with the same medium. Moreover, the time dependence appearing in (3.13) does not figure anymore, because the value obtained from the central static is used throughout the calculation, as already said.

The static calculations are meant to compute fission spectra and initialize flux values for the following dynamic simulation. The latter demands a specific treatment for the delayed fission source (3.14) which leads us to consider, for each temporal point of the period, contributions due to all other instants. The next paragraph aims to show this aspect.

3.2.1 Delayed-term treatment

In section 3.1 we said that the frequency model is based on the hypothesis that criticality is preserved during the perturbation. This assumption is not present in our work, but the solution sought is still an asymptotic dynamic equilibrium and deviations from the initial criticality are to be taken into account to guarantee this equilibrium; how this is made is explained in 3.2.4, whereas here we discuss about the implications of this strategy on the delayed term.

In condition of asymptotic equilibrium, if our system undergoes a periodic oscillation of cross sections due to physical shifts of structural components, per-family precursor concentrations are also periodic, with period T equal to the oscillation period. In order

¹Here we mean by “medium” each set of different cross-section values. This difference can be due to material composition, but also to numerical and modelization reasons such as the subdivision of fuel regions in different shielding zones.

to take advantage of this periodicity, eq. (3.17) is firstly integrated over time, yielding

$$C_i(\vec{r}, t) = C_i(\vec{r}, 0) e^{-\lambda_i t} + \int_0^t dt' e^{-\lambda_i(t-t')} \sum_j \int_E dE' w_{d,i}^j P_{ed}^j(E') \nu \Sigma_{f,j}(\vec{r}, E', t') \phi(\vec{r}, E', t'). \quad (3.21)$$

Solving (3.21) for $t = T$, one obtains an expression for $C_i(\vec{r}, 0)$ which can be substituted in the same equation. This leads to the final version of our precursor equation:

$$C_i(\vec{r}, t) = \int_0^T dt' \left(\frac{e^{-\lambda_i T}}{1 - e^{-\lambda_i T}} + \theta_{[0,t]} \right) e^{-\lambda_i(t-t')} \sum_j \int_E dE' w_{d,i}^j P_{ed}^j(E') \nu \Sigma_{f,j}(\vec{r}, E', t') \phi(\vec{r}, E', t'), \quad (3.22)$$

where $\theta_{[0,t]}$ is equal to 1 if $t' \in [0, t]$, to 0 otherwise. Therefore, the delayed source (3.14) can be rewritten as

$$\begin{aligned} & \sum_i \bar{\chi}_i^D(\vec{r}, E) \lambda_i C_i(\vec{r}, t) = \\ & \sum_i \bar{\chi}_i^D(\vec{r}, E) \lambda_i \int_0^T dt' \left(\frac{e^{-\lambda_i T}}{1 - e^{-\lambda_i T}} + \theta_{[0,t]} \right) e^{-\lambda_i(t-t')} \\ & \sum_j \int_E dE' w_{d,i}^j P_{ed}^j(E') \nu \Sigma_{f,j}(\vec{r}, E', t') \phi(\vec{r}, E', t'). \end{aligned} \quad (3.23)$$

As anticipated above, the solution of the problem at time t clearly depends on the system behaviour during an entire period, because of the integral over time present in the last formula. This also permits to consider, instead of the original coupled kinetic system made by (3.16) and (3.17), just the transport equation where no variable appears apart from the flux. To implement (3.23) into the right-hand side of (2.18) that is, at the outer-iteration level of the algorithm discussed in 2.4, a quadrature formula is needed that translates the time integral into a weighted sum.

3.2.2 Quadrature formula for the delayed source

In order to translate in a numerical form the fission source, the time period is discretized in N uniform sub-intervals, each one identified by the index k and centred around the instant $t_k = (k - 1/2) \frac{T}{N}$. The chosen value for N is 8 for both cases that will be described in 3.3. The delayed fission source is therefore approximated by a quadrature formula of the kind

$$\sum_i \bar{\chi}_i^D(\vec{r}, E) \lambda_i \sum_{k'=1}^N w_{i,k}(t_{k'}) \sum_j \int_E dE' w_{d,i}^j P_{ed}^j(E') \nu \Sigma_{f,j}(\vec{r}, E', t_{k'}) \phi(\vec{r}, E', t_{k'}) \quad (3.24)$$

$w_{i,k}(t_{k'})$ being the k' -th weighting coefficient for delayed family i at time t_k ; this means that for each pair (i, t_k) a new set of weights has to be computed, corresponding to all the

points of the period. For consistency, from the hypothesis we have made about precursor concentrations it follows that also the flux has to be a T -periodic function. Therefore, the sum over fissile isotopes \sum_j present in (3.24) is also T -periodic. Taking into account this fact we want our weights to preserve the analytical value of the integral with any T -periodic function in place of the sum, up to a given order of approximation. This can be done up to a certain frequency, depending on the available time steps. The integrals we want to conserve are therefore the following:

$$\int_0^T dt' \left(\frac{e^{-\lambda_i T}}{1 - e^{-\lambda_i T}} + \theta_{[0,t]} \right) e^{-\lambda_i(t-t')} e^{i_u \frac{2\pi n}{T} t'}, \quad n = 0, N/2, \quad (3.25)$$

whose analytical solutions are

$$\frac{\lambda_i \cos\left(\frac{2\pi n}{T} t\right) + \frac{2\pi n}{T} \sin\left(\frac{2\pi n}{T} t\right)}{\lambda_i^2 + \frac{4\pi^2 n^2}{T^2}} + i_u \frac{\lambda_i \sin\left(\frac{2\pi n}{T} t\right) - \frac{2\pi n}{T} \cos\left(\frac{2\pi n}{T} t\right)}{\lambda_i^2 + \frac{4\pi^2 n^2}{T^2}}, \quad n = 0, N/2. \quad (3.26)$$

i_u is again the imaginary unit and n an integer number determining the frequency n/T of the periodic function that appears in the integral. Since $e^{i_u \frac{2\pi n}{T} t'} = \cos\left(\frac{2\pi n}{T} t'\right) + i_u \sin\left(\frac{2\pi n}{T} t'\right)$, it follows that the real part of (3.26) is due to the cosine contribution, while the imaginary part to the sine one. For this reason and to obtain one and only one solution for the weighting coefficients, an equation for sines and one for cosines are to be considered for each value of n apart from 0 and $N/2$; for the latter we have decided to write a sine equation, whereas the former leads to an equation with unit coefficients. Globally, the number of equation for weights is equal to that of time steps. An $\mathcal{A}\vec{w}_{i,k} = \vec{b}_{i,k}$ system has to be solved, where $\vec{w}_{i,k}$ is the unknown vector of the N weights for the pair (i, t_k) , matrix \mathcal{A} is constructed as

$$\mathcal{A} = \begin{bmatrix} 1 & 1 & 1 & \dots & 1 \\ \sin\left(\frac{2\pi}{T} t_1\right) & \sin\left(\frac{2\pi}{T} t_2\right) & \sin\left(\frac{2\pi}{T} t_3\right) & \dots & \sin\left(\frac{2\pi}{T} t_N\right) \\ \cos\left(\frac{2\pi}{T} t_1\right) & \cos\left(\frac{2\pi}{T} t_2\right) & \cos\left(\frac{2\pi}{T} t_3\right) & \dots & \cos\left(\frac{2\pi}{T} t_N\right) \\ \sin\left(\frac{4\pi}{T} t_1\right) & \sin\left(\frac{4\pi}{T} t_2\right) & \sin\left(\frac{4\pi}{T} t_3\right) & \dots & \sin\left(\frac{4\pi}{T} t_N\right) \\ \vdots & \vdots & \vdots & \ddots & \vdots \\ \sin\left(\frac{2\pi N/2}{T} t_1\right) & \sin\left(\frac{2\pi N/2}{T} t_2\right) & \sin\left(\frac{2\pi N/2}{T} t_3\right) & \dots & \sin\left(\frac{2\pi N/2}{T} t_N\right) \end{bmatrix}$$

and $\vec{b}_{i,k}$ contains the analytic values of the integrals, arranged as follows:

$$\vec{b}_{i,k} = \begin{bmatrix} \frac{1}{\lambda_i} \\ \frac{\lambda_i \sin\left(\frac{2\pi}{T} t_k\right) - \frac{2\pi}{T} \cos\left(\frac{2\pi}{T} t_k\right)}{\lambda_i^2 + \frac{4\pi^2}{T^2}} \\ \frac{\lambda_i \cos\left(\frac{2\pi}{T} t_k\right) + \frac{2\pi}{T} \sin\left(\frac{2\pi}{T} t_k\right)}{\lambda_i^2 + \frac{4\pi^2}{T^2}} \\ \frac{\lambda_i \sin\left(\frac{4\pi}{T} t_k\right) - \frac{4\pi}{T} \cos\left(\frac{4\pi}{T} t_k\right)}{\lambda_i^2 + \frac{16\pi^2}{T^2}} \\ \vdots \\ \frac{\lambda_i \sin\left(\frac{2\pi N/2}{T} t_k\right) - \frac{2\pi N/2}{T} \cos\left(\frac{2\pi N/2}{T} t_k\right)}{\lambda_i^2 + \frac{4\pi^2(N/2)^2}{T^2}} \end{bmatrix}$$

Computing the weights in this way is equivalent to say that, if our periodic function were equal to $\sum_{n=0}^{N/2-1} [c_{2,n} \cos\left(\frac{2\pi n}{T} t\right) + c_{1,n} \sin\left(\frac{2\pi n}{T} t\right)] + c_{1,N/2} \sin\left(\frac{2\pi N/2}{T} t\right)$, with $c_{1,n}$ and $c_{2,n}$ arbitrary constant values, our approximation would be exact.

3.2.3 Adiabatic approximation

Differently from the frequency approach, our method does not need to make any assumption on the magnitude of the oscillations: a priori, cross sections may undergo variations of any entity and frequency, without compromising the method. As for the oscillation frequency, we always consider the value 1Hz, in order to remain within the framework of mechanical vibrations [13]. In light of this, something can be said about the time-derivative term figuring in (3.16): the classical numerical strategy to deal with derivatives is the Finite Difference Method, which translates the derivative into a ratio of finite terms. With a central difference scheme, the approximation reads

$$\frac{1}{v(E)} \frac{\partial \psi(\vec{r}, \vec{\Omega}, E, t)}{\partial t} \approx \frac{N[\psi(\vec{r}, \vec{\Omega}, E, t_{k+1}) - \psi(\vec{r}, \vec{\Omega}, E, t_{k-1})]}{2Tv(E)}. \quad (3.27)$$

Since the neutron velocity v takes quite high values also in the thermal domain (about 220 000 cm/s for 0.025 eV neutrons), for relatively long periods one may think of neglecting this term: this strategy is adopted in our work.

3.2.4 Eigenvalue update

Provided that no external source is present, all the terms of Boltzmann equation are operators acting on the flux, constituting therefore a homogeneous problem. As such, it is certainly satisfied by the trivial null solution. The existence of other solutions requires the total operator applied to the flux to be singular: to this aim, we re-write eq. (3.16) by inserting a k_{eff} parameter to force dynamic criticality. Our new problem will be

$$\left(\mathcal{L}(t) - \mathcal{H}(t)\right)\psi(t) = \frac{1}{k_{eff}}\mathcal{F}(t)\phi(t) \quad (3.28)$$

and the k_{eff} will be searched on the base of the condition that

$$\int_T dt \langle \mathcal{F}(t)\phi(t) \rangle = const, \quad (3.29)$$

where “ $\langle \dots \rangle$ ” denotes the integration over phase spaces. That is to say that the fission integral along the period will be constant over time.

The eigenvalue problem produces a stationary solution for the flux which does not describe reality; however, by considering the k_{eff} value one can infer which the system behaviour would be. If the eigenvalue is not equal to 1 (that is, if the system is not critical) feedback effects can be introduced to establish criticality and make the flux solution the real one. In this sense, an eigenvalue different from 1 can be seen as a fictitious feedback acting on the system to maintain the dynamic equilibrium between neutron production and removal.

Even if starting from a critical condition, neutron noise may be responsible for more or less relevant insertions of reactivity, alternately positive and negative. This may lead the number of fission reactions to diverge or to decrease progressively up to be negligible, depending on the value of the average reactivity along a period; however, even if this latter is equal to 0, the presence of delayed neutrons may be promoter of system divergence, as described for a point reactor in [11]. In our case, in order to preserve an asymptotic periodic behaviour, any deviation from an average 0 value for the reactivity is compensated with the eigenvalue by which the fission source is divided. In the light of what said in section 3.2.1 and considering how the k_{eff} is updated after each outer iteration (2.21), our eigenvalue takes into account the entire evolution of the system during the period and is therefore suitable for this task. Fig. 3.2 shows the algorithm we have adopted for computing and updating until convergence the dynamic k_{eff} and the fission source values over time. For the former, the relative error between successive iterates has to be less or equal to $1.0 \cdot 10^{-5}$, whereas for the latter the maximum acceptable value for the relative error over the period has been set to $2.0 \cdot 10^{-4}$.

3.3 Description of studied systems

The described method has been implemented for two different 2-D geometries; the oscillation motions, however similar, required a specific modelling for each of them, due

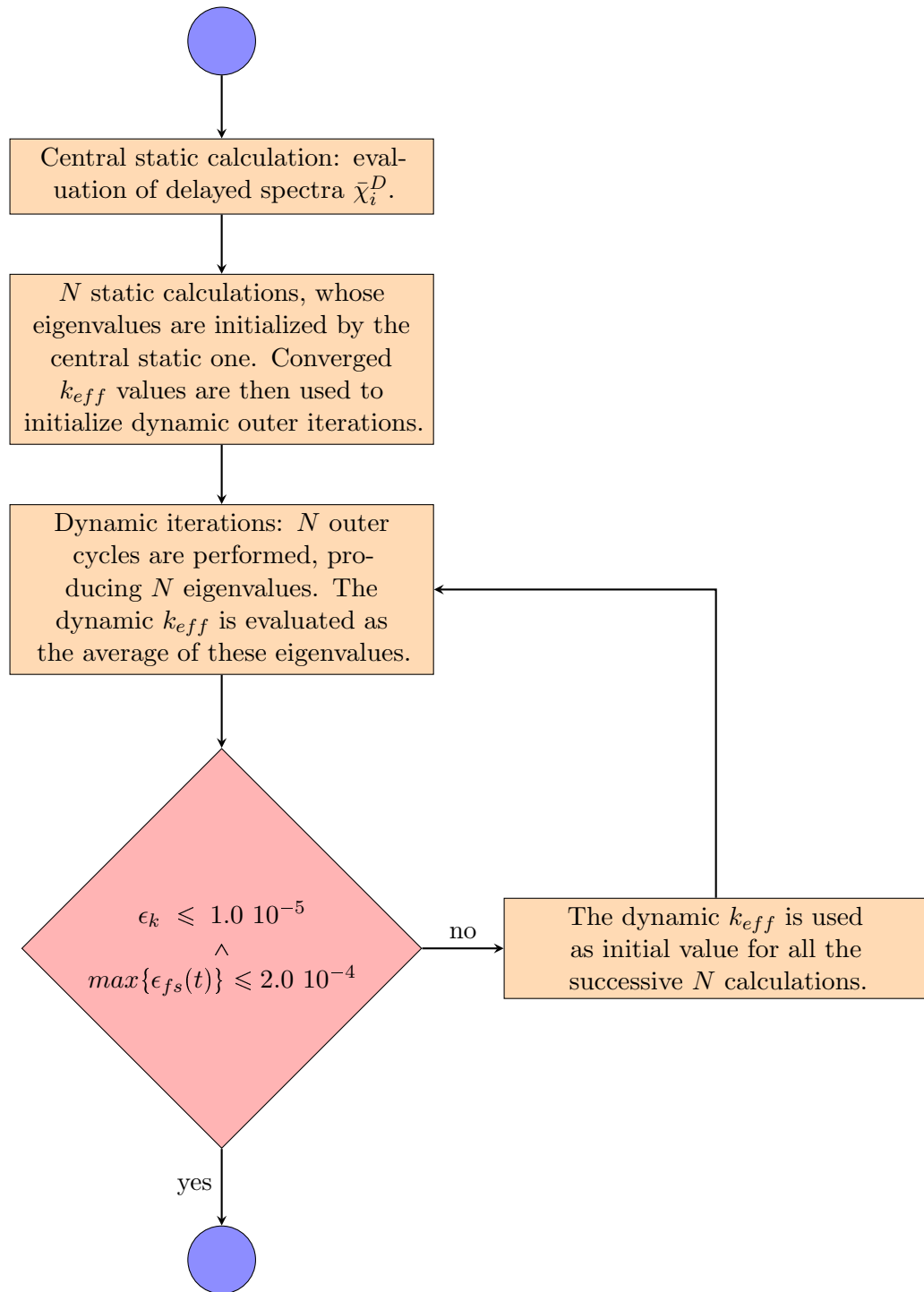


Figure 3.2: Algorithm for noise iterations. ϵ_k and ϵ_{f_s} are the relative errors between successive iterations of the dynamic k_{eff} and of the fission sources $\langle \mathcal{F}(t)\phi(t) \rangle$, respectively. For the latter, the maximum value over the period is considered to check convergence.

Table 3.2: Values of relevant dimensions for the two cases. Shift amplitudes are referred to the centre of mass of the moving components.

Dimensions		cm
Cell side		1.26502
Fuel cladding outer radius		$4.75988 \cdot 10^{-1}$
Control-rod cladding radius		$4.86125 \cdot 10^{-1}$
Detector	shift amplitude	$5.80000 \cdot 10^{-1}$
	anode radius	$1.50000 \cdot 10^{-1}$
	cathode outer radius	$2.00000 \cdot 10^{-1}$
	envelope outer radius	$2.80000 \cdot 10^{-1}$
Rod assembly	shift amplitude	$2.32016 \cdot 10^{-1}$

to the different structural components involved. Their most relevant dimensions can be found in Tab. 3.2. The conditions imposed at the boundary are pure reflective for both cases: this is equivalent to have an infinite system and to study only a portion of it, since this latter repeats an infinite number of times to constitute the global system. As already said, this kind of boundary condition is used for fine lattice calculations and it is a good assumption if a power reactor sub-system like a fuel cell or an assembly is considered, because it is actually surrounded by a large number of similar, if not equal, elements. Unfortunately, the same cannot be said in our case: imposing that the oscillation takes place in a sub-system implies the symmetric oscillation of infinite other sub-systems, which is clearly unrealistic. A way to limit the problem would be to consider larger sub-systems, so that the effects of the neighbours on the one studied would be minimized (at least in the zone close to the noise source); of course, this would require much higher simulation performances, certainly excessive compared to those available during the internship. Therefore, for these first uses of our noise method we have decided to still adopt reflective conditions. Possible consequences of this choice on our results will be discussed in chapter 5.

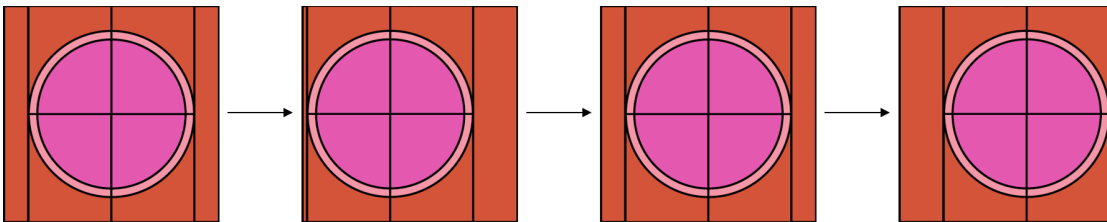


Figure 3.3: Simulation of the oscillation. The geometries are linked in order to represent the period of motion. The example considers $N = 4$ (in our cases we used 8 time intervals) and shows only one of the cells where the oscillation takes place.

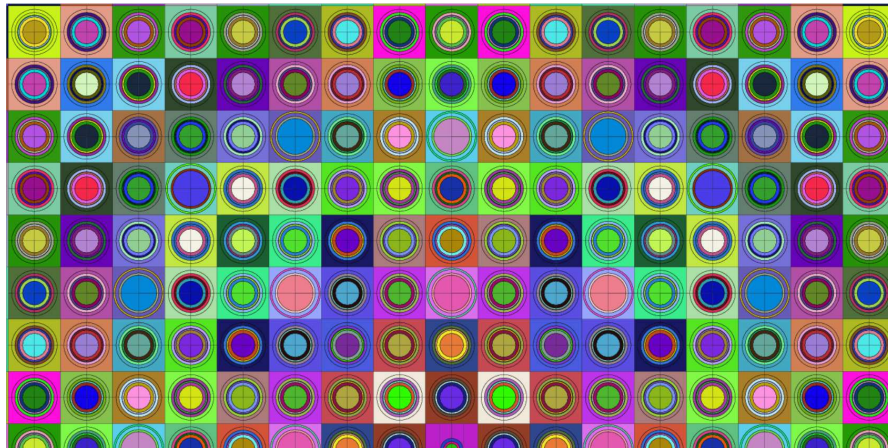


Figure 3.4: *Case study 1 - detector. The oscillating component is in the central cell (the first row down for the halved domain).*

Before considering the two case studies individually, it is necessary to specify how the sequence of geometries constituting the oscillation period is generated: each of the N sub-intervals is associated to a distinct geometry, that is, to a different position of the component. The oscillation is therefore constructed linking properly these static geometries, as shown in Fig. 3.3 for $N = 4$.

In both cases temperatures are considered as fixed and equal to 841.00 K in the fuel and to 579.55 K in all the other components.

3.3.1 Case 1: detector

The first case considered is shown in Fig. 3.4: it is a 17x17 fuel assembly with boron control rods inserted containing, inside the water tube at its centre, a three-layer cylinder constituting a fission chamber, that is, a detector useful to obtain in-core flux measurements. The three layers are the following, from the outside in:

envelope the shielding component preventing the radiations from reaching the coolant;

cathode containing uranium (only 235 in our case); here fission reactions take place with the aim of generating charged particles through radioactive decay and ionizations;

anode needed to establish a current between it and the cathode by applying a potential difference. This current should be proportional to the reaction rates and, therefore, to the flux.

They are all made of an iron-nickel-chromium alloy containing also manganese, silicon and cobalt; uranium oxide is present only in the cathode. In PWRs (Pressurized Water Reactors) this instrument is usually inserted from above, by means of a structure which is only fixed at the top; it follows that the detector is left free to move, potentially swinging in its available space. Such an oscillation is what has been simulated, with the

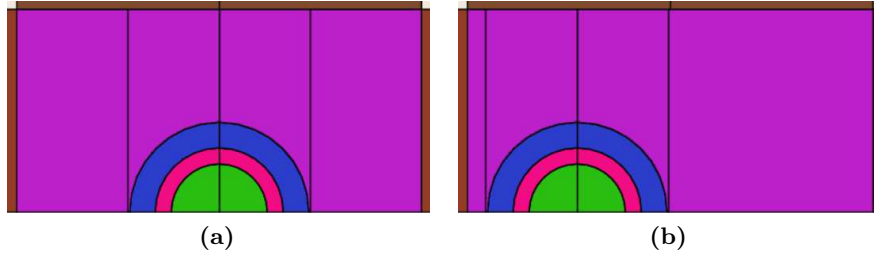


Figure 3.5: *Detector oscillation. The central static (a) and the leftmost position (b) are shown. The motion takes place along the entire diameter of the water tube.*

fission chamber moving along the diameter of the water tube section. The scope of our procedure is to highlight the effects of this motion on the fission rate inside the detector, as it is the key phenomenon for its operation. Since we only deal with 2-D configurations, this analysis is based on the assumption that the detector is actually made by a cylinder of infinite height; hence, any relevant effect on fission rates of neighbouring fuel rods may be due to this hypothesis.

In Fig. 3.4 it is apparent that only half of the domain is shown; this is not a casual choice, but a direct consequence of the studied motion, shown in Fig. 3.5: a horizontal oscillation determines an identical behaviour in the upper and lower halves, and this implies that the portion of the system shown is sufficient for its complete description. In the same figure one can also see that the detector is not surrounded by any water tube, as in reality would be: in fact, it has been removed to simplify the simulation, and the elements of which it is composed have been dissolved in the water around the detector. Moreover, this latter is considered to move within the space which would be available if the tube were actually present.

The nuclear fuel contained in all fuel cells (not in the detector) is 1.8% enriched uranium.

3.3.2 Case 2: control-rod assembly

The other system analysed is a cluster of 9 fuel assemblies, arranged on a 3x3 grid, where in the central one control rods are inserted (Fig. 3.6). Each assembly is, as in the previous case, composed of 289 cells. Considering again PWRs, it is well-known that control assemblies are inserted from the top of the core and that, during normal operation, are always partially inserted. Our 2-D study, however, is more similar to the behaviour of a mid-height section of the core when rods are fully inserted, because, as already said, it supposes that we are in an infinite axially extruded geometry.

Due to the turbulent motion of the coolant flowing across the core, one may hypothesize that control rods move too. This movement may occur in several ways, but in this work simply a coherent oscillation of the entire control assembly, composed of 24 rods, is assumed to take place: this means that at the same time all the control rods move leftwards and rightwards alternately. This is shown in Fig. 3.7.

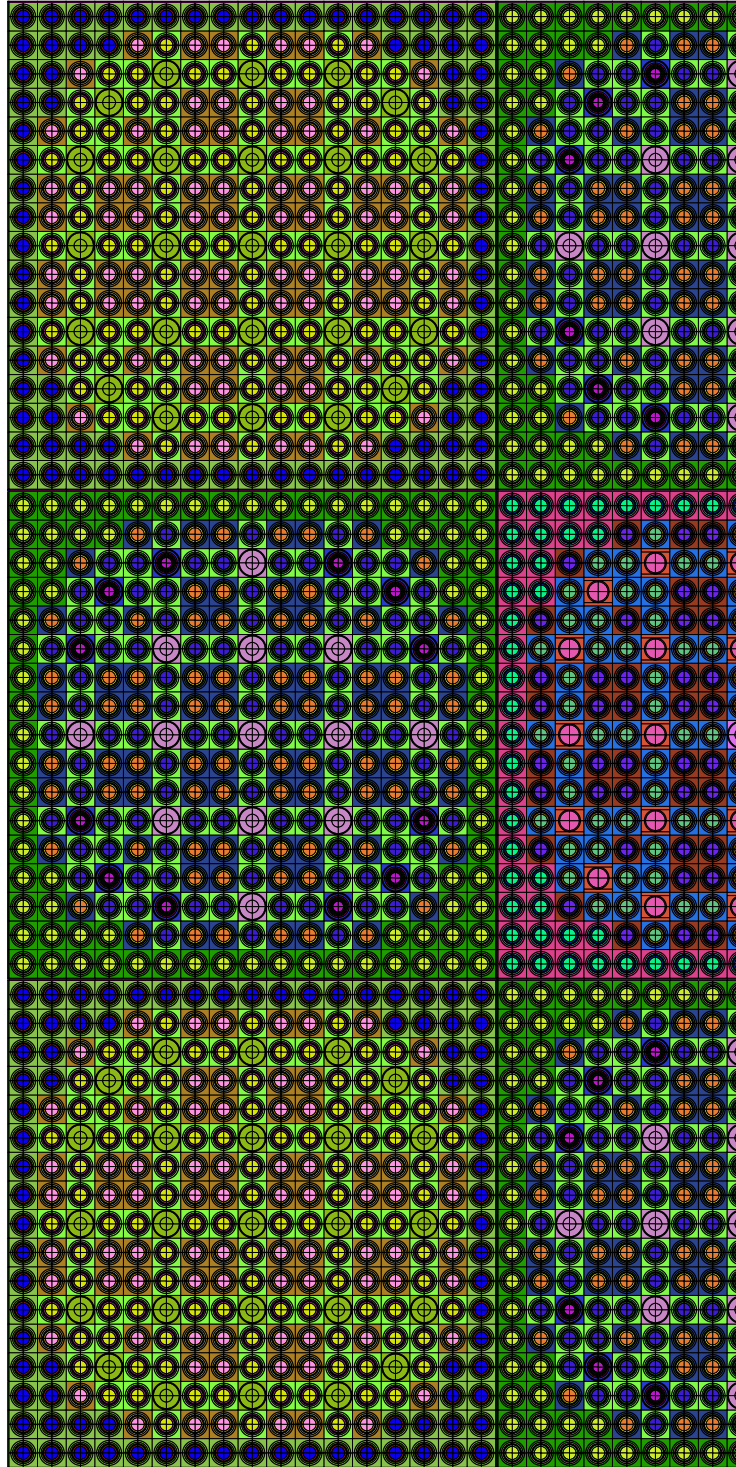
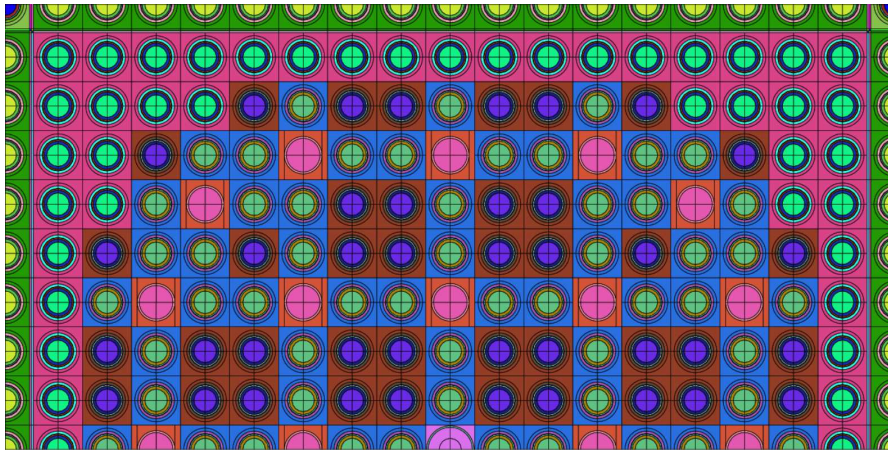
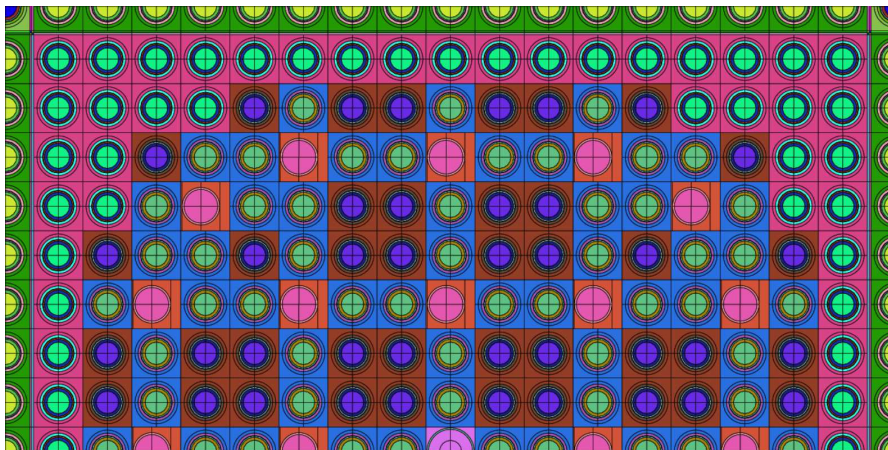


Figure 3.6: *Case study 2 - control-rod assembly. The halved domain is shown rotated 90 degrees with respect to the oscillation direction. The moving control rods are in the central assembly.*



(a)



(b)

Figure 3.7: Control-rod oscillation. The central static (a) and the leftmost position (b) are shown. The motion takes place along the entire diameter of guide tubes.

Analogously to what done for case 1, only half of the domain has been considered. Moreover, around each rod a guide tube is present in real systems, preventing the contact with the fuel (especially in accidental situations, when structural deformations may hinder control-rod insertion); here again the guide tubes are dissolved in the water surrounding the rods.

Each of the four fuel assemblies sharing one side with the central one contains 9 pyrex rods, made of borosilicate burnable absorber material. In these assemblies 2.4% enriched uranium is employed, while for the others the enrichment is 1.8%. The other control rods are made of natural boron.

3.4 A model for neutron leakage

To conclude this chapter dedicated to the description of our method we illustrate the leakage model. In order to increase the representativeness of our approach we have in fact used this traditional tool to simulate the impact of the finite reactor size over lattice calculations. The model described in this section is based on [15].

Starting from any heterogeneous domain, in order to have $k_{eff} = 1$ one may think of modifying the streaming term of the transport equation accordingly, either increasing or lowering neutron leakages from the system. This task is simplified by considering a homogeneous medium, equivalent to the initial heterogeneous one, for which a leakage coefficient is computed assuming that it remains valid for the heterogeneous case. This strategy is called “homogeneous leakage approximation”, and the assumption it is based on is reasonable if the system anisotropy is not too pronounced: for instance, in PWRs there are for sure anisotropic effects due to the vertical disposition of the fuel, but they are traditionally neglected in 2-D models.

First, we want to show how the leakage coefficient appears for an infinite homogeneous and isotropic critical medium. In this case, the transport equation reads

$$(\vec{\Omega} \cdot \nabla + \Sigma_t)\psi = q, \quad (3.30)$$

where

$$q(\vec{r}, \vec{\Omega}, E) = \int_E dE' \int_{S_{\vec{\Omega}}} d\Omega' \Sigma_s(\vec{\Omega}' \cdot \vec{\Omega}, E' \rightarrow E)\psi(\vec{r}, \vec{\Omega}', E') + \frac{1}{4\pi}(\mathcal{F}\phi)(\vec{r}, E),$$

$$(\mathcal{F}\phi)(\vec{r}, E) = \sum_j \chi_j(E) \int_E dE' (\nu\Sigma_{f,j})(E')\phi(\vec{r}, E'). \quad (3.31)$$

The flux solution is to be found in the form

$$\psi(\vec{r}, \vec{\Omega}, E) = \psi(\vec{B}, \vec{\Omega}, E)e^{-i_u \vec{B} \cdot \vec{r}}, \quad (3.32)$$

\vec{B} being the buckling vector. Hence, eq. 3.30 translates into

$$[\Sigma_t(E) - i_u \vec{B} \cdot \vec{\Omega}]\psi(\vec{B}, \vec{\Omega}, E) = q(\vec{B}, \vec{\Omega}, E). \quad (3.33)$$

Some comments can be made about the relation between \vec{B} , ψ and the current \vec{J} : the isotropy of the medium implies that the flux and the module of the current depend only on the module of \vec{B} (because they do not vary if \vec{B} and $\vec{\Omega}$ rotate simultaneously). Moreover, it follows from (3.33) that \vec{B} and $\vec{J}(B, E)$ have the same direction, since the dependency of the angular flux on \vec{B} is limited to the product $\vec{B} \cdot \vec{\Omega}$. According to these considerations, by integrating eq. (3.33) over angles the conservation equation is obtained in the form

$$i_u B J(B, E) - \Sigma_t(E) \phi(B, E) + Q(B, E) = 0. \quad (3.34)$$

Defining now a coefficient D as

$$D(B, E) = -\frac{i_u J(B, E)}{B \phi(B, E)}, \quad (3.35)$$

from (3.34) the real flux $\phi(\vec{r}, E)$ turns out to be solution of the multi-group diffusion equation

$$[D(B, E) \nabla^2 - \Sigma_t(E)] \phi(\vec{r}, E) + Q(\vec{r}, E) = 0 \quad (3.36)$$

having (3.35) as diffusion coefficient.

Considering now the original heterogeneous problem, we would like to introduce a leakage coefficient defined as D for the homogeneous case. To do that the following factorization for the flux ψ_R is adopted:

$$\psi_R(\vec{r}, \vec{\Omega}, E) = f(\vec{r}) \psi(\vec{r}, \vec{\Omega}, E), \quad (3.37)$$

f being the macroscopic flux, result of the material balance over the entire core, and ψ the local one, affected by variations of cross sections on a local scale (fuel cell, assembly or cluster). Therefore, the transport equation can be written as

$$\left[\vec{\Omega} \cdot \left(\nabla + \frac{\nabla f}{f} \right) + \Sigma_t \right] \psi = q \quad (3.38)$$

which, integrated over angles, reads

$$\left(\nabla + \frac{\nabla f}{f} \right) \cdot \vec{J}(\vec{r}, E) + \Sigma_t \phi(\vec{r}, E) = Q(\vec{r}, E), \quad (3.39)$$

where only the dependencies of the new terms are shown. At this point, the homogeneous leakage approximation is introduced: first, the macroscopic flux is assumed of the form $e^{-i_u \vec{B} \cdot \vec{r}}$, as in an infinite homogeneous medium, so that $\frac{\nabla f}{f} = -i_u \vec{B}$; then, one supposes that the r.h.s. of this last relation can be expressed by means of (3.35), that is, using a coefficient independent of the spatial position (hence the name of ‘‘homogeneous’’ leakages) and of the angle. The approximation, reading

$$\frac{\nabla f}{f} \cdot \vec{J} \approx DB^2 \phi, \quad (3.40)$$

can therefore be substituted in (3.39). This latter is integrated over the chosen “local” spatial domain of volume V_D to give its homogenized version:

$$(-DB^2 - \Sigma_{t,D})\phi_D(E) + Q_D(E) = V_D^{-1} \int_{\delta D} d\vec{S} \cdot \vec{J}(\vec{r}, E). \quad (3.41)$$

The subscript D refers to average volumetric values and $\Sigma_{t,D}$ results from the homogenization made by the flux. Considering that the current is null on a perfectly reflective boundary, Eq. (3.41) acquires the same form of (3.36): it therefore describes the behaviour of a homogeneous medium equivalent to the real one. As can be seen, DB^2 , that is the product of the leakage coefficient and the critical buckling, modifies the total cross section in order to have a critical system (it can be thought of as an additional absorption section).

The procedure to implement this model in our code is iterative, because the homogenized cross sections, needed to evaluate the leakage coefficient, depend on the heterogeneous flux, which in turn depends on the leakages. The required steps can be summarized as follows:

- 1** update of homogenized cross sections relative to the equivalent homogeneous medium;
- 2** evaluation of the homogenous leakage coefficient;
- 3** evaluation of the critical buckling;
- 4** introduction of DB^2 into the cross sections (total or scattering);
- 5** update of the heterogeneous flux.

This cycle has to be repeated until k_{eff} converges to the unit value.

The leakage coefficient and the critical buckling are computed only for the central static configuration, to ensure that noise actually starts from a critical condition, and are therefore used for all temporal points.

Chapter 4

Acceleration method

The iteration scheme described in 2.4, usually referred to as “free iterations” [1], may converge to the solution rather slowly: there is therefore a need to adopt acceleration techniques that reduce the computational time. For this purpose, two different strategies have been used at the same time: firstly, a special treatment is reserved to the fission source, due to its expression in our temporal noise problem; secondly, a DP_N synthetic acceleration is implemented. It has to be noted that these techniques apply to each time step of the noise period: the acceleration of our method is achieved by accelerating the convergence of single period points.

This chapter deals with the description of the two tools mentioned and aims to show the acceleration performance (and need) by comparing simulation times for a simpler noise problem.

4.1 Wielandt scheme for outer iterations

The starting point is eq. (3.16) which, in the light of our manipulations and hypotheses, can be compactly expressed as

$$(\mathcal{L} - \mathcal{H})\psi(t) = \frac{1}{k_{eff}} \left[\mathcal{F}_P\phi(t) + (\mathcal{F}_D\vec{\phi})(t) \right], \quad (4.1)$$

where the dependence of the delayed term on the values of the flux over the period is highlighted by the vector notation. The meaning of the eigenvalue k_{eff} for our kinetic problem has been discussed in 3.2.4; from now on, it will be referred to simply as k . Considering the eigenvalue problem

$$\mathcal{A}\phi = (\mathcal{M}^{-1}\mathcal{F})\phi = k\phi \iff \mathcal{M}\phi = \frac{1}{k}\mathcal{F}\phi, \quad (4.2)$$

having exactly the same form as (4.1), the number of power iterations to reach the convergence of the fundamental eigenvector depends on the so-called “dominance ratio” σ , equal to the ratio $\frac{k_2}{k_1}$ of the two highest eigenvalues k_2 and k_1 of matrix $\mathcal{M}^{-1}\mathcal{F}$ (k_1 being the fundamental one). In particular, the smaller σ and the faster the convergence.

As proposed for example in [23], the value of the dominance ratio can be reduced by means of an eigenvalue shift, modifying the original problem as follows:

$$\left(\mathcal{M} - \frac{1}{k_s}\mathcal{F}\right)\phi = \left(\frac{1}{k} - \frac{1}{k_s}\right)\mathcal{F}\phi. \quad (4.3)$$

This procedure is called Wielandt shift method, and in order for the shift to be effective k_s must be greater than k_1 : in this way the new dominance ratio, given by

$$\sigma' = \frac{k'_2}{k'_1} = \frac{\frac{1}{k'_1}}{\frac{1}{k'_2}} = \frac{\frac{1}{k_1} - \frac{1}{k_s}}{\frac{1}{k_2} - \frac{1}{k_s}}, \quad (4.4)$$

is surely smaller than the initial one. In our work a sort of Wielandt scheme has been implemented by subtracting the prompt source to both sides of (4.1): the resulting iterative equation is therefore

$$(\mathcal{L} - \mathcal{H})\psi^o(t_k) - \frac{1}{k^{o-1}}\mathcal{F}_P\phi^o(t_k) = \frac{1}{k^{o-1}}(\mathcal{F}_D\vec{\phi}^{o-1})(t_k), \quad k = 1, N. \quad (4.5)$$

Comparing the previous equation with (4.3), clearly $\frac{1}{k_s}\mathcal{F}\phi \rightarrow \frac{1}{k}\mathcal{F}_P\phi$. It follows that

$$\frac{k}{k_s} = \frac{\mathcal{F}_P\phi}{\mathcal{F}\phi}, \quad (4.6)$$

where the right-hand side is equal to the fraction of prompt neutrons ($\sim 99.4\%$ for thermal systems). If the reactivity oscillation due to noise is small compared to the 600 pcm of difference between total and thermal sources, our fictitious k_s is always greater than the dynamic eigenvalue. As this is the case, our procedure reduces the dominance ratio, leading to a faster convergence. To update the eigenvalue the condition is to re-scale the delayed emission with the help of the estimated eigenvalue as

$$k^o = k^{o-1} \frac{\|\mathcal{F}_D\vec{\phi}^o\|}{\|\mathcal{F}_D\vec{\phi}^{o-1}\|}, \quad (4.7)$$

the norm indicating the integral over the phase space.

4.2 DP_N synthetic acceleration

According to the Wielandt scheme just described, each outer iteration contains within it a further level of fixed-source iterations, like:

$$(\mathcal{L} - \mathcal{H})\psi^{s-f}(t_k) = \frac{1}{k^{o-1}}\mathcal{F}_p\phi^{s-1}(t_k) + S^{o-1}(t_k), \quad k = 1, N, \quad (4.8)$$

where the index s denotes the nested iteration level. Provided the initial criticality and because of the prompt-delayed separation, eq. (4.8) identifies a sub-critical source problem for all time steps: a physical result is therefore expected to be found. For a

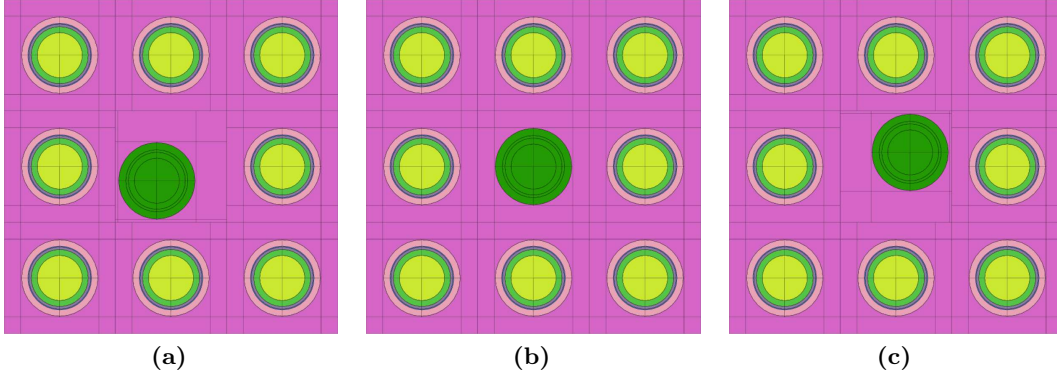


Figure 4.1: *Small case for performance comparison. The control rod oscillates along the diagonal of the cell. (a) and (c) are the most distant positions from the centre, which is shown in (b).*

full transport solution f in the left-hand side is equal to 0, but to further accelerate our procedure we have coupled it with the synthetic acceleration method implemented in TDT: the DP_N scheme. Initially proposed by Sanchez and Chetaine in [14], it is meant to solve a problem derived from the original one considering also the converged solution, denoted by “ ∞ ”:

$$(\mathcal{L} - \mathcal{H})\psi^\infty(t_k) = \frac{1}{k^{o-1}}\mathcal{F}_p\phi^\infty(t_k) + S^{o-1}(t_k), \quad k = 1, N. \quad (4.9)$$

By indicating with $\frac{1}{2}$ the value of f for the latest transport solution, $\psi^{s-\frac{1}{2}}$, and with

$\delta\phi^{s-\frac{1}{2}} = \phi^\infty - \phi^{s-\frac{1}{2}}$ the error affecting the $(s - \frac{1}{2})^{th}$ transport iteration ($\delta\psi^{s-\frac{1}{2}}$ for the angular flux),

$\Delta\phi = \phi^{s-\frac{1}{2}} - \phi^{s-1}$ the difference between the current transport solution and the iterate relative to the previous step,

one can subtract eq. (4.8) to (4.9) to obtain

$$(\mathcal{L} - \mathcal{H})\delta\psi^{s-\frac{1}{2}}(t_k) - \frac{1}{k^{o-1}}\mathcal{F}_p\delta\phi^{s-\frac{1}{2}}(t_k) = \frac{1}{k^{o-1}}\mathcal{F}_p\Delta\phi(t_k), \quad k = 1, N. \quad (4.10)$$

The aim is to compute $\delta\phi$ and to add it to the latest transport solution in order for the next iterate $\phi^s = \phi^{s-\frac{1}{2}} + \delta\phi^{s-\frac{1}{2}}$ to be a better estimation of the real solution. However, problem (4.10) is as difficult as the original one: as it is, this strategy would not lead to any advantage. The acceleration is therefore made on a simplified problem, where the transport operator \mathcal{L} is replaced by a low-order one, \mathcal{L}_{DP_N} . According to [17], this substitution is based on two approximations: the former regards the number of angular moments considered, which is here reduced; the latter treats the region boundary as a set of surfaces, and for the boundary fluxes of each surface only surface-averaged

Table 4.1: Comparison free-accelerated. The eigenvalues and the times required by the simulations are shown.

	Iterations	
	free	accelerated
Eigenvalue	0.73827	0.73820
CPU time [s]	22621	4978

(hence spatially constant) angular moments are used. In this way the chord dependence of the MOC, assuming constant angular fluxes over the cross-sectional area of each trajectory, is lost to the advantage of computational cost. On both surface sides the angular dependence is expressed by means of a P_N spherical-harmonic expansion: hence, a “Double P_N ” expansion is adopted, giving the name to the acceleration method.

4.3 Performance comparison

In order to show the effectiveness of the acceleration a small case is considered, whose domain is composed of a 3x3 grid of cells. In the central cell a control rod is present which oscillates as shown in Fig. 4.1, while the other cells contain fuel. As for the detector and the control-assembly cases, the rod is made of natural boron; the fuel is 1.8% enriched uranium. The side of each cell is 1.28885 cm and the movement of the control rod, which takes place along the diagonal of the cell with a period of 0.2 s, has an amplitude of 0.66178 cm.

In Tab. 4.1 one can see the converged eigenvalues and the computation times relative to the case of “free iterations” and to the accelerated one. The former differ by less than 10 pcm, which is a rather acceptable quantity, especially considering that the acceleration reduces the simulation time by 78%.

Time interval	Fission integral
1	0.73302
2	1.12530
3	1.34575
4	1.12978
5	0.73304
6	1.12398
7	1.34570
8	1.12855

Table 4.2: Fission integrals over time.

# static	Eigenvalue
1	0.73572
2	0.73839
3	0.73918
4	0.73839
5	0.73572
6	0.73839
7	0.73918
8	0.73839

Table 4.3: Static eigenvalues.

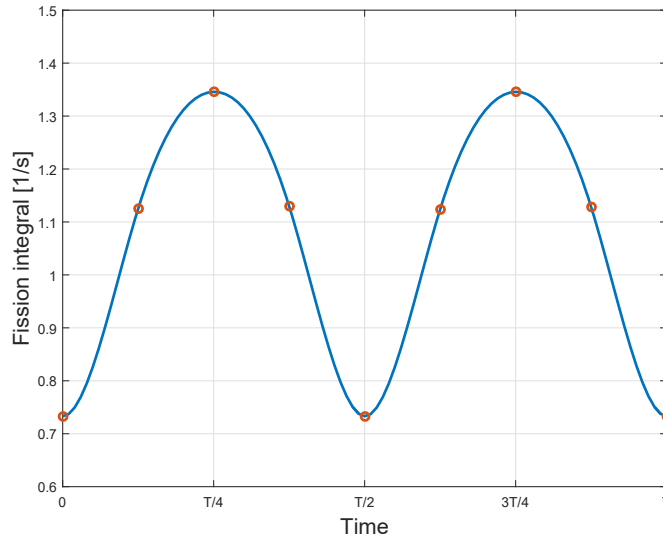


Figure 4.2: *Fission integral oscillation along the period. The red points correspond to the measured values of Tab. 4.2, which are interpolated by the cubic blue line.*

Another interesting aspect of this simple case is to see how the fission integral over the whole domain D , given by

$$I_F(t) = \sum_{j=1, N_{isotopes}} \int_D d\vec{r} \int_E dE \nu \Sigma_{f,j}(\vec{r}, E, t) \phi(\vec{r}, E, t), \quad (4.11)$$

oscillates along the period: the values are reported in Tab. 4.2 and plotted in Fig. 4.2. The amplitude of this variation reaches 56.57% of the average value. However, such a high oscillation is very different from what we have obtained for the two main case studies (see chapter 5): this can be due to the big difference among the eigenvalues of the static configurations of this case, which alternately produces a relevant insertion of positive and negative reactivity. Tab. 4.3 contains these values: clearly, the leakage model discussed in 3.4 has not been adopted here.

Chapter 5

Results

In this chapter we will show the effects of the oscillation, that is to say, the neutron noise itself, on a fundamental quantity for nuclear engineering: the number of fission reactions occurring per unit time in a certain spatial domain. Thanks to the fission rates we can compute the power density, by taking into account the energy released by each fission reaction.

Before looking at fission rates, we intend to show the extent of the oscillation with respect to the effective multiplication factor. Given an initial critical condition (the central static), Tab. 5.3 contains k_{eff} values of the 8 static configurations studied (shown in Tab. 5.1 and 5.2) alongside with the dynamic one, for each case. The period starts from the non-oscillation position and develops up to the leftmost position first and then to the rightmost one, before returning to the centre. These two most distant configurations correspond to the highest k_{eff} -variation. The static values allow us to predict the effect of the noise on the average behaviour of the system along the period (indicated by the dynamic k_{eff}): considering the smallness of the fluctuation for both cases, we were expecting the dynamic values not to be far from criticality, as indeed they are.

Such a small oscillation was a desirable result for the detector case: the unavoidable movement of the fission chamber must not affect the surrounding system, as long as a significative measurement is to be performed. In this sense, although limited to a 2-D infinite geometry, our simulation confirms the validity of using this kind of instrument for in-core detection (this point will be discussed again later, when fission rates are involved). On the other hand, unexpectedly the shift of a whole control assembly modifies quite weakly the global state, as the k_{eff} amplitude of oscillation is no more than 3 pcm of the central static value. A possible explanation may be linked to the domain structure: the purely reflective boundary generates an infinite heterogeneous system where one assembly every 9 contains moving control rods, and this may lead to a compensation effect between neighbouring assemblies. In future works following our strategy, to compute more realistically the neutron noise for such cases we suggest to reduce or even to exclude these kinds of effects: to that end, huge computational resources would be needed that we did not have available for the present thesis.

Table 5.1: Positions of the detector along the period. Δx is referred to the centre of the cell.

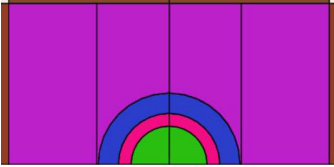
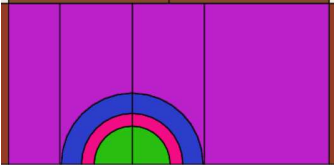
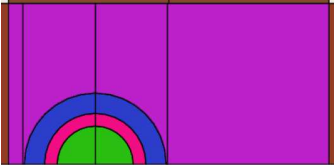
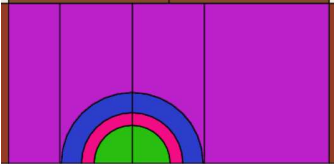
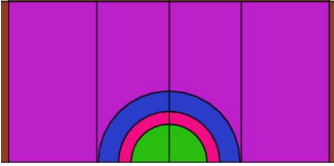
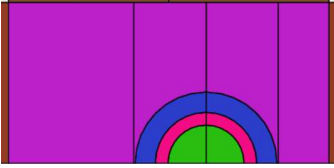
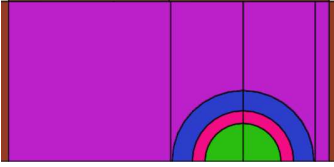
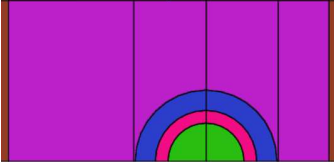
Sub-interval	Position	Δx [cm]
1		0
2		$-1.45 \cdot 10^{-1}$
3		$-2.90 \cdot 10^{-1}$
4		$-1.45 \cdot 10^{-1}$
5		0
6		$+1.45 \cdot 10^{-1}$
7		$+2.90 \cdot 10^{-1}$
8		$+1.45 \cdot 10^{-1}$

Table 5.2: Positions of each control rod of the central assembly along the period. Δx is referred to the centre of the cell.

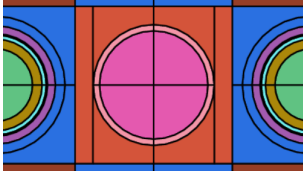
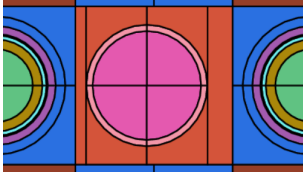
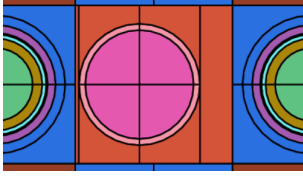
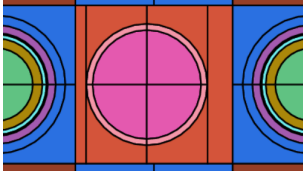
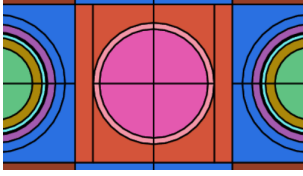
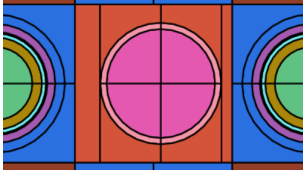
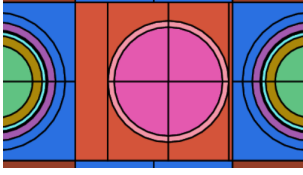
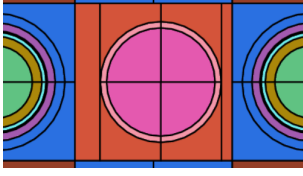
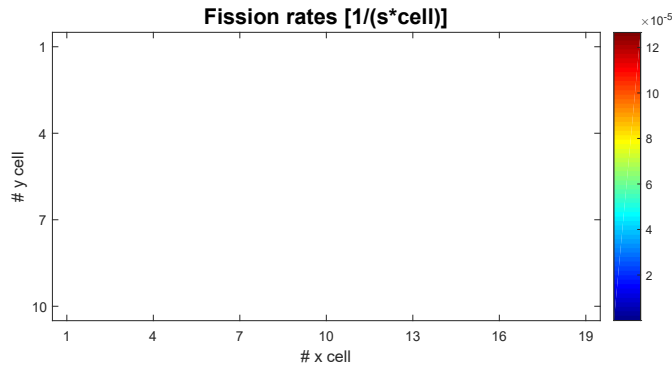
Sub-interval	Position	Δx [cm]
1		0
2		$-5.80 \cdot 10^{-2}$
3		$-1.16 \cdot 10^{-1}$
4		$-5.80 \cdot 10^{-2}$
5		0
6		$+5.80 \cdot 10^{-2}$
7		$+1.16 \cdot 10^{-1}$
8		$+5.80 \cdot 10^{-2}$

Table 5.3: k_{eff} values and number of noise iterations (see Fig. 3.2) for the two cases.

	k_{eff}	
	detector	control rods
central static	1.00000	1.00000
statics	1	1.00001
	2	1.00002
	3	1.00003
	4	1.00002
	5	1.00001
	6	1.00002
	7	1.00003
	8	1.00002
dynamic	1.00005	0.99996
# noise iterations	2	4

**Figure 5.1:** Fission rates for the detector case described in 3.3.1.

5.1 Fission-rate analysis

We focus now on fission rates which are, at least from an industrial point of view, a more interesting quantity. Denoting by V_i the volume of the general fuel cell i , the fission rate τ_i relative to the same cell can be expressed, as a function of time, as

$$\tau_i(t) = \int_{V_i} d\vec{r} \int_E dE \Sigma_f(\vec{r}, E, t) \phi(\vec{r}, E, t). \quad (5.1)$$

Some comments have to be made about the flux dependency in (5.1): for an infinite medium the value of the flux cannot be determined unequivocally as the eigenfunctions of the transport problem, but it depends on an arbitrary normalization. It follows that, without this last operation, fission rates may assume any value (maintaining the proper

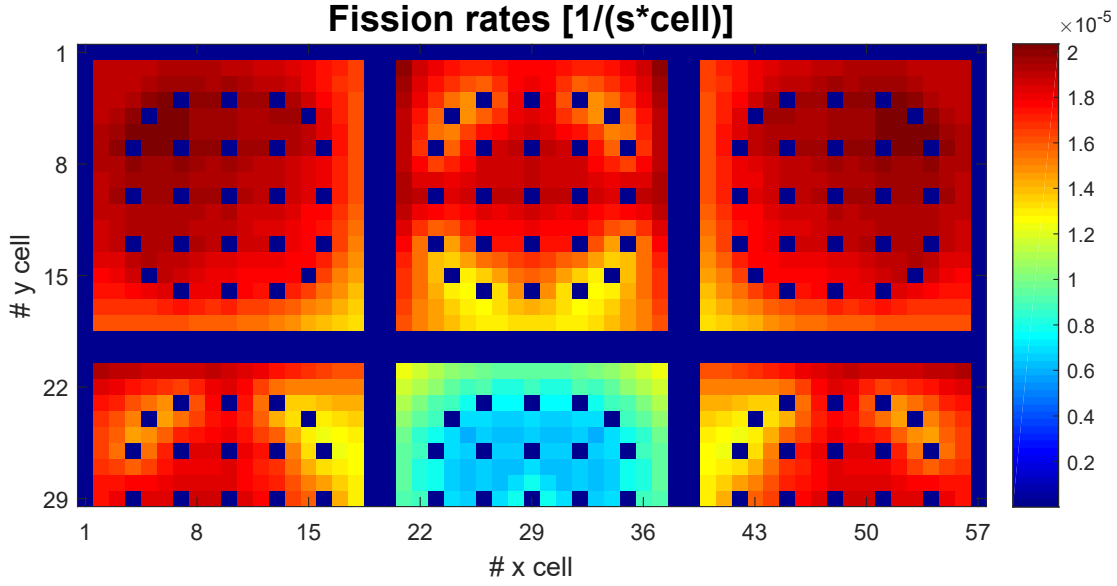


Figure 5.2: *Fission rates for the cluster case described in 3.3.2.*

proportions between different spatial positions), even far from realistic results. This is shown in Fig. 5.1 and 5.2. Luckily enough, it does not prevent us from making an analysis in relative terms, which is what interests in the noise field.

Due to the structural periodic shifts of the detector and the control assembly, fission rates acquire a periodic behaviour with the same period, attributable to local variations in the moderating ratio (defined as the ratio between moderator and fuel volumes). We are interested in studying deviations with respect to the average value over the period for each cell: identifying it as $\bar{\tau}_i$ and as τ_i^{max} and τ_i^{min} the maximum and minimum values over the period, respectively, one can define a maximum relative deviation as

$$\left(\frac{\delta\tau}{\tau}\right)_i = \frac{1}{\bar{\tau}_i} \max\{(\tau_i^{max} - \bar{\tau}_i); (\bar{\tau}_i - \tau_i^{min})\}. \quad (5.2)$$

In the following the distribution of this quantity over the domain will be shown for our two cases. In order to better highlight the noise effect, a very small concentration of fissile material (uranium 235) is dissolved in the water. This leads us to measure the highest relative deviations in the cells containing the moving structures. It must be said that the occurrence of fission reactions within the coolant is surely unphysical and that this is only useful for graphic purposes.

5.1.1 Detector

For the first case the maximum amplitude of oscillation is in the central cell, as predictable, where the detector is inserted. As shown in Fig. 5.3 and 5.4, the peak corresponds to 0.983% of the average fission rate. While in the direction perpendicular

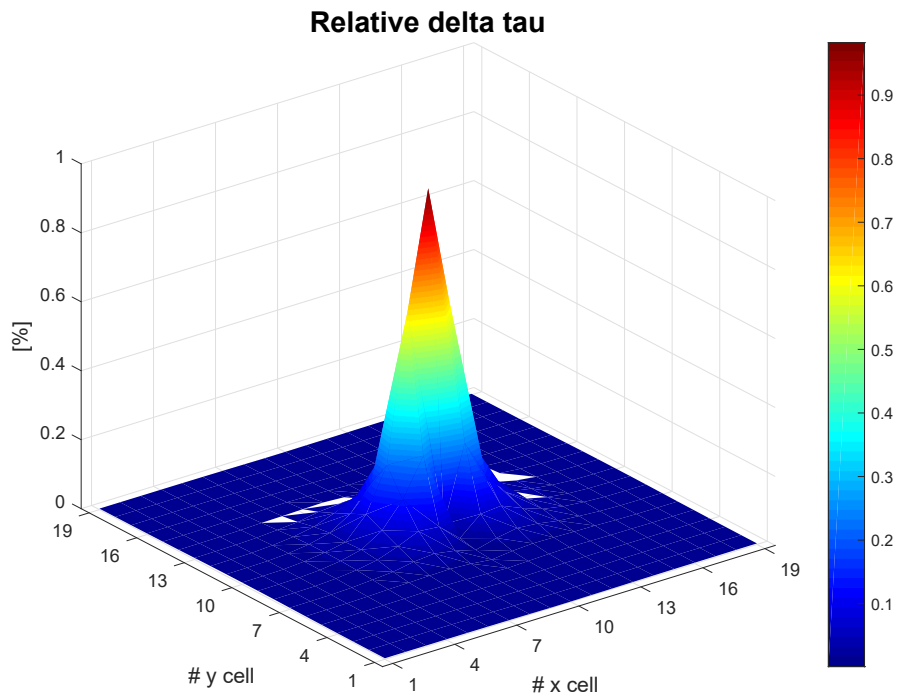


Figure 5.3: *Detector relative delta tau. The entire domain, symmetric with respect to the x-axis, is plotted to better show the result. The central peak corresponds clearly to the detector cell, for which the relative delta tau is equal to 0.983%.*

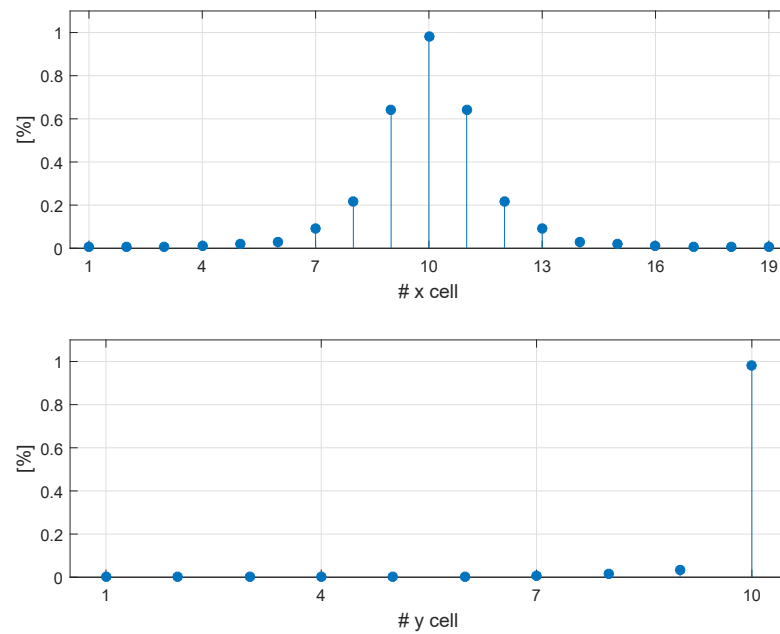


Figure 5.4: *Detector relative delta tau along the x-axis (above) and y-axis (below).*

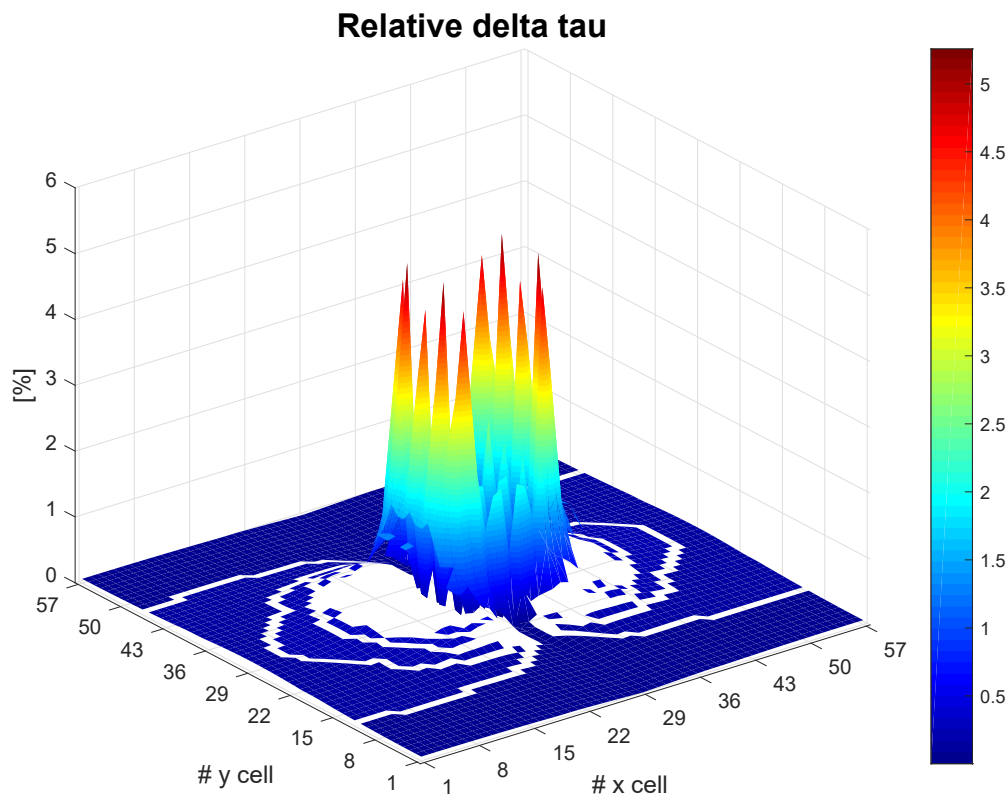


Figure 5.5: Cluster relative delta tau. As in Fig. 5.3, the whole domain is considered. It is apparent how the most external control rods are the most perturbed, together with the neighbouring fuel cells.

to the detector motion the amplitude is soon attenuated (it is already equal to 0.033% in the fuel cells next to the detector), the same cannot be said for the parallel direction: an attenuation occurs, but only to 0.643% on the right and on the left of the detector. This value denies in part what said with respect to the k_{eff} variation, since one cannot accept such a high perturbation during an in-core measurement. However, this may be due to the approximation we have adopted for the detector dimensions: in fact, the 2-D model entails an infinite height of the detector, which may be the reason why excessive amplitudes are obtained. Our results thus show the need for a 3-D model for a correct study of the noise generated by the detector insertion.

5.1.2 Control-rod assembly

As long as neutron noise is regarded, the cluster case is much more interesting: the movement of the control rods along the whole diameter of the guide tubes causes in fact an oscillation of considerable amplitude. This can be seen in Fig. 5.5, 5.6 and 5.7, where the highest values correspond to the cells containing the moving rods (as already

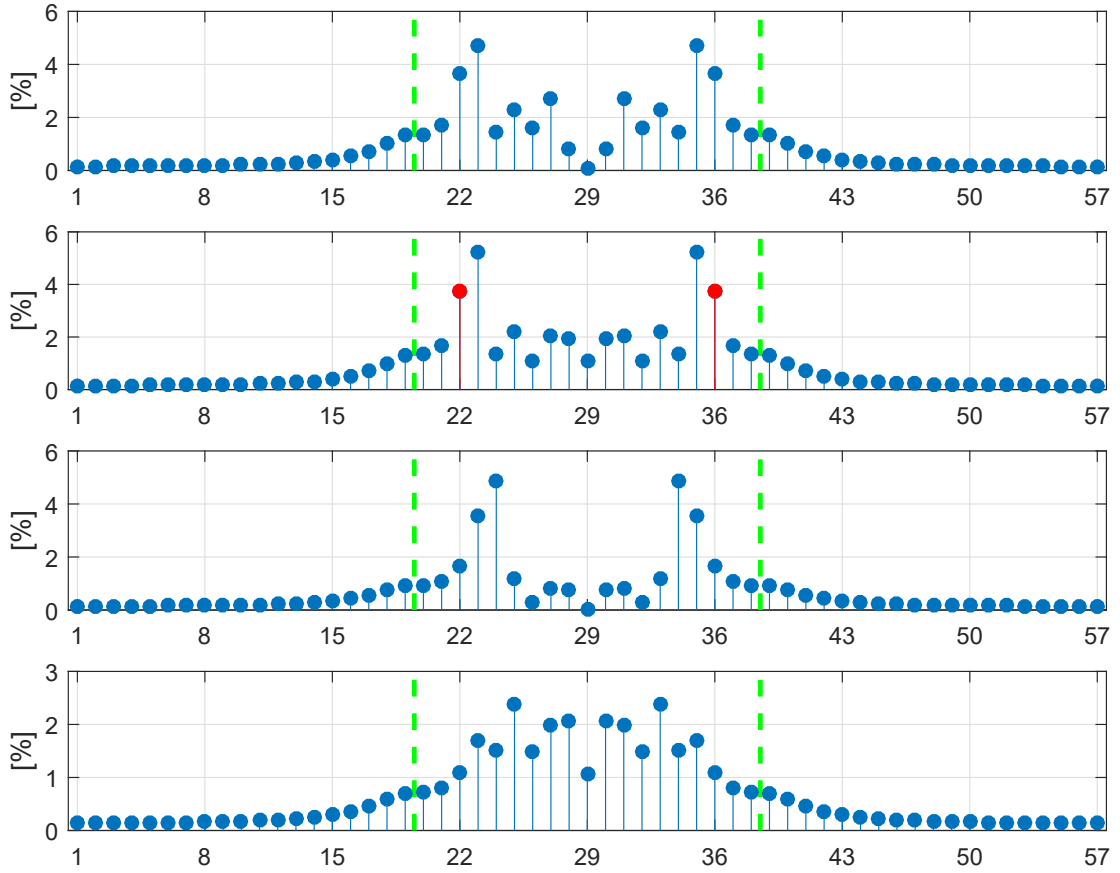


Figure 5.6: From top to bottom, cluster relative delta tau along the x-axis and rows 26, 24 and 23. The two red values correspond to the most perturbed fuel cells, while dashed green lines are used to mark the separation between different assemblies.

said, their noise is fictitious). As in the previous case, the system is mostly perturbed along the direction of the rod motion: exiting the central assembly in the perpendicular direction no cell has an amplitude higher than 1%. The region enclosed by the moving rods shows generally remarkable levels of noise, reaching 2.720% along the x-axis (this latter is also the symmetry axis, with respect to which our halved domain can be doubled to retrieve the original cluster). However, the highest amplitudes are obtained outside the rods, in the two (four in the real domain) fuel cells of coordinates (22,26) and (36,26). Here the maximum relative variation of the fission rate reaches 3.719%, which can be regarded as the most relevant result of the present work.

Notwithstanding the values obtained for the assembly containing the moving rods, the effect of the noise is clearly limited to this same assembly: the perturbation in the left and right assemblies exceeds 1%, but only in the first row of cells. As it is apparent from Fig. 5.5, the attenuation is so strong that the six assemblies above and below the central one are practically unaffected by the oscillation. As said for the k_{eff} behaviour, this

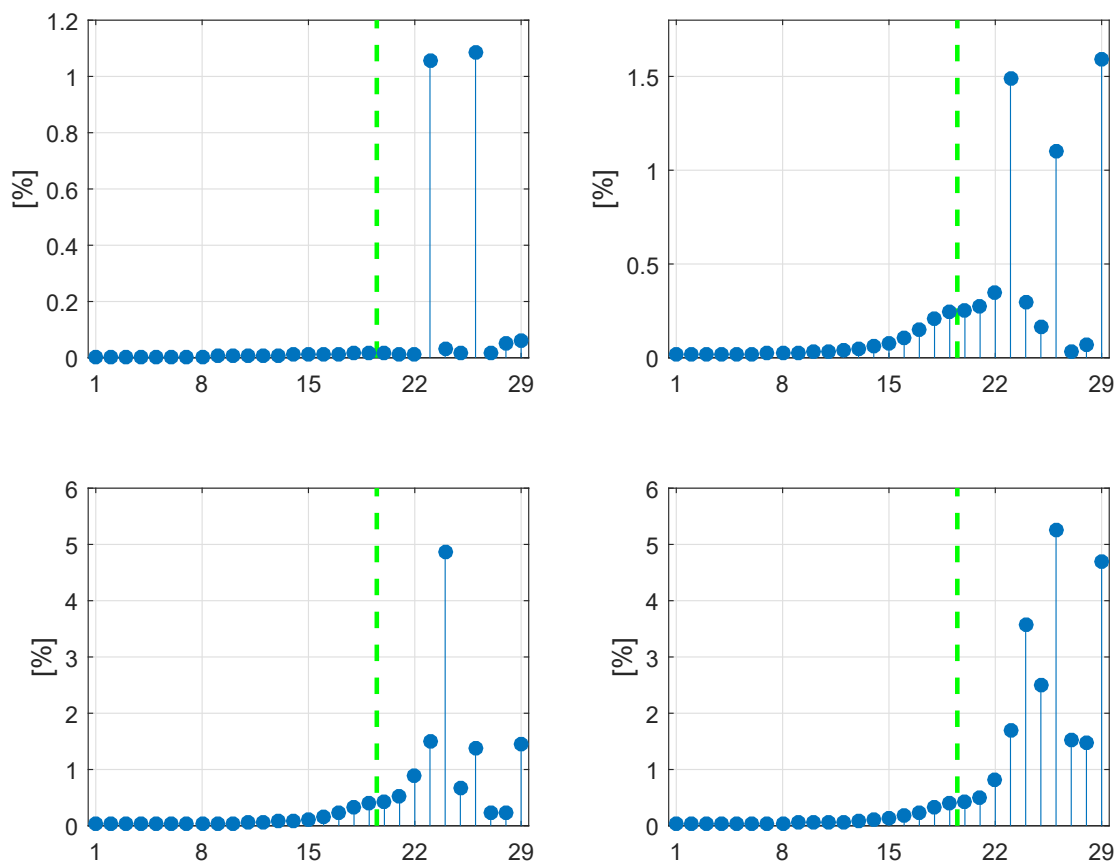


Figure 5.7: Cluster relative delta tau along the y -axis (top-left) and columns 26 (top-right), 24 (bottom-left) and 23 (bottom-right). The dashed green lines have the same purpose as those in Fig. 5.6, that is, to signal assembly separation.

result may be due to the boundary conditions: the infinite heterogeneous medium can be imagined as composed of infinite rows, perpendicular to the rod shifting, where for each couple of adjacent rows the control rods move in phase but in the opposite direction. Therefore, the further we move away from the rods of a cluster the stronger the effect of those of the next cluster is. This attenuation and/or compensation also prevents us from any attempt of performing a phase shift analysis: in fact, moving away from the noise source one would expect to obtain little changes in the oscillation phase, but in our case this is hindered by the very low noise measured far from the moving rods (to the point that neutron noise gets confused with the numerical one).

In any case, the computed fluctuation of the rod assembly is interesting twofold: on one side, the absence of macroscopic effects of the oscillation on reactivity is coherent with the observed behaviour of real systems; on the other side our calculation shows the presence of measurable and important local flux fluctuations that can impact on the thermo-mechanical system response.

Chapter 6

Conclusions

In this work we have conceived and implemented in the reactor code system APOLLO3[®] a noise model which simulates the oscillation of structural components and analyses its effects on reactivity and fission rates. Under the hypothesis of periodicity, the positions over time of the detector and of the control rods are identified by different geometries, which are then linked in the proper order to construct the oscillation period. Following this procedure, noise is studied within the real temporal domain, without the need of Fourier transforming and of the small-perturbation hypothesis used in the traditional frequency-based approach.

The fission source of delayed neutrons required a specific treatment, which led us to express it as a function of the flux values over all the period and, by discretizing the latter in a finite number of sub-intervals, to evaluate the time integral by a quadrature formula suitable for periodic functions.

Each noise iteration is made by a set of outer iterations (one per temporal sub-interval) and updates the dynamic eigenvalue relative to the whole period as the average of the instantaneous values, until the convergence of this value and of each fission source over the period.

Two acceleration strategies, the Wielandt shift scheme and the DP_N synthetic acceleration, are combined to achieve a faster convergence of the noise iterations, which is obtained accelerating the outer iterations relative to each temporal point. Applied to a small case, this strategy proved to be effective in significantly reducing the computation time.

Looking at our results, the oscillations produce a relevant noise with regard to fission rates: in particular, for the control-rod case the amplitude reaches 3.719% of the period average value (much higher values are found in the cells containing the oscillating rods, suggesting greater local flux variations). The reactivity is much less affected, as the deviation of the dynamic eigenvalue from the static situation is practically insignificant, at least to nuclear engineering. This is somehow a reassuring result, since field experience has never shown evident effects on reactivity due to vibrating components. On the other hand, the limits of our computational resources inevitably impact the likelihood of our model: the 2-D domains hardly resemble reality, especially for the detector case, where

an object of some centimetres is inserted in a system a few meters high. The control assembly model is instead more realistic, as long as the rods are assumed as fully inserted. The boundary conditions constitute probably an even worse issue: reflectivity produces infinite domains that oscillate in phase, so that our noise source actually repeats over and over. This may be the reason why our noise looks so attenuated in so little space, that is, because of a compensation effect among neighbouring assemblies.

In conclusion, the temporal noise model shows significant fluctuations of per-cell fission rates, suggesting the possibility of detecting structure vibrations by analyzing variations of the local flux. Better and more realistic results could be obtained in future works by considering larger and even 3-D geometries, which would make it possible to simulate the effect of the oscillation in a single cell or assembly on a relevant portion of a reactor and, potentially, on its totality.

Appendix A

Complex and real spherical harmonics

The dependence on the angular variable is traditionally addressed by expanding the terms of Boltzmann equation over spherical harmonics, which are complex functions defined as follows [3]:

$$Y_k^m(\vec{\Omega}) = \sqrt{\frac{2k+1}{4\pi} \frac{(k-m)!}{(k+m)!}} P_k^m(\mu) e^{im\varphi}, \quad (\text{A.1})$$

i being the imaginary unit, $k = 0, 1, \dots, +\infty$ and $m \in [-k, k]$. The other terms call for more explanation:

- $\vec{\Omega}$ is the direction vector (shown in Fig. A.1) which can be expressed as a function of the polar angle $\theta \in [-\frac{\pi}{2}, \frac{\pi}{2}]$ and the azimuthal angle $\varphi \in [0, 2\pi)$:

$$\vec{\Omega} = \sqrt{1-\mu^2} \cos \varphi \hat{e}_x + \sqrt{1-\mu^2} \sin \varphi \hat{e}_y + \mu \hat{e}_z, \quad (\text{A.2})$$

where μ is equal to $\cos \theta$ and \hat{e}_x , \hat{e}_y and \hat{e}_z are the unit vectors of cartesian coordinates;

- $P_k^m(\mu)$ is the associated Legendre function, defined as ¹,

$$P_k^m(\mu) = \left(\sqrt{1-\mu^2}\right)^m \frac{d^m P_k(\mu)}{d\mu^m}, \quad (\text{A.3})$$

$P_k(\mu)$ being the k^{th} Legendre polynomial, whose definition is

$$P_k(\mu) = \frac{1}{2^k k!} \frac{d^k}{d\mu^k} (\mu^2 - 1)^k. \quad (\text{A.4})$$

¹Here we have followed the convention, adopted for instance in [6], which does not insert the phase factor $(-1)^m$. This term is however present in [3], that is the classical text this appendix is based on.

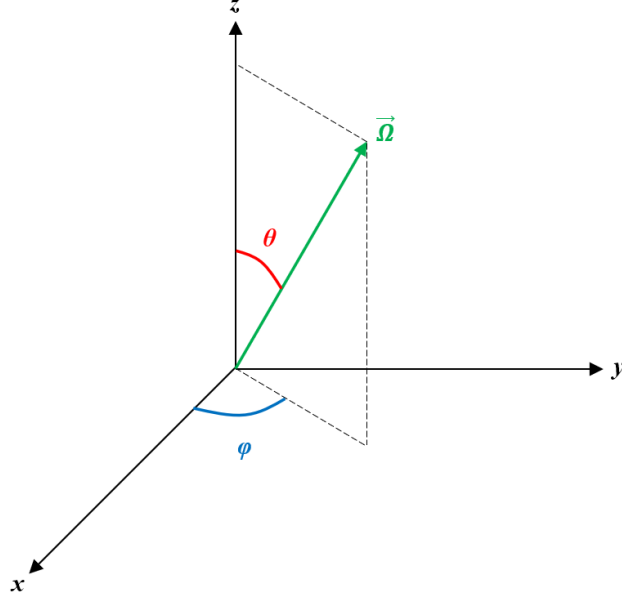


Figure A.1: The direction vector $\vec{\Omega}$. The dependence of the angular variable on polar and azimuthal angles is here shown.

It can be shown that (A.3) and (A.4) imply the following relation for P_k^{-m} :

$$P_k^{-m}(\mu) = \frac{(k-m)!}{(k+m)!} P_k^m(\mu), \quad (\text{A.5})$$

from which it follows that $Y_k^{-m} = Y_k^{m*}$, where $*$ denotes the complex conjugate.

The complex spherical harmonics are orthonormal, since

$$\int_{S_{\vec{\Omega}}} d\Omega Y_k^m(\vec{\Omega}) Y_{k'}^{m'*}(\vec{\Omega}) = \delta_{kk'} \delta_{mm'}, \quad (\text{A.6})$$

$\delta_{kk'}$ and $\delta_{mm'}$ being Kronecker deltas, and complete, because any function $f(\vec{\Omega})$ can be expanded into an infinite sum of terms as

$$f(\vec{\Omega}) = \sum_{k=0}^{+\infty} \sum_{k=-m}^m f_k^m Y_k^m(\vec{\Omega}), \quad (\text{A.7})$$

with

$$f_k^m = \int_{S_{\vec{\Omega}}} d\Omega f(\vec{\Omega}) Y_k^{m*}(\vec{\Omega}). \quad (\text{A.8})$$

They constitute therefore an orthonormal base in $S_{\vec{\Omega}}$ (whereas Legendre polynomials are an orthonormal base in $[-1,1]$).

According to the addition theorem, valid for spherical harmonics,

$$P_k(\vec{\Omega}' \cdot \vec{\Omega}) = \frac{4\pi}{2k+1} \sum_{m=-k}^k Y_k^{m*}(\vec{\Omega}') Y_k^m(\vec{\Omega}). \quad (\text{A.9})$$

This gives us the opportunity to introduce the real spherical harmonics. Thanks to (A.5), the last relation can in fact be re-written as

$$P_k(\vec{\Omega}' \cdot \vec{\Omega}) = \sum_{m=-k}^k A_k^m(\vec{\Omega}') A_k^m(\vec{\Omega}), \quad (\text{A.10})$$

by defining the real spherical harmonics A_k^m :

$$A_k^m(\vec{\Omega}) = \begin{cases} \sqrt{(2 - \delta_{0m}) \frac{(k-m)!}{(k+m)!}} P_k^m(\mu) \cos(m\varphi) & m \geq 0 \\ \sqrt{2 \frac{(k-m)!}{(k+m)!}} P_k^m(\mu) \sin(m\varphi) & m < 0 \end{cases} \quad (\text{A.11})$$

These functions are preferred to the complex ones because they are of course simpler to handle; as the former, they represent a complete base in $S_{\vec{\Omega}}$, but are “only” orthogonal, since

$$\int_{S_{\vec{\Omega}}} d\Omega A_k^m(\vec{\Omega}) A_{k'}^{m'}(\vec{\Omega}) = \frac{4\pi}{2k+1} \delta_{kk'} \delta_{mm'}. \quad (\text{A.12})$$

Similarly to (A.7), one can write

$$f(\vec{\Omega}) = \sum_{k=0}^{+\infty} \sum_{k=-m}^m f_k^m A_k^m(\vec{\Omega}), \quad (\text{A.13})$$

where

$$f_k^m = \frac{2k+1}{4\pi} \int_{S_{\vec{\Omega}}} d\Omega f(\vec{\Omega}) A_k^m(\vec{\Omega}). \quad (\text{A.14})$$

Bibliography

- [1] ADAMS M. L., LARSEN E. W., 2002, *Fast iterative methods for discrete-ordinates particle transport calculations*, Progress in Nuclear Energy 40, 3-159.
- [2] ASKEW J. R., 1972, *A characteristics formulation of the neutron transport equation in complicated geometries*, Report AEEW-M 1108, United Kingdom.
- [3] BELL G. I., GLASSTONE S., 1970, *Nuclear Reactor Theory*, Van Nostrand Reinhold, New York, USA.
- [4] COMMISSARIAT À L'ÉNERGIE ATOMIQUE ET AUX ÉNERGIES ALTERNATIVES, 2013, *La neutronique*, LE MONITEUR, Paris, France.
- [5] FRY D. N., 1971, *Experience in reactor malfunction diagnosis using on-line noise analysis*, Nuclear Technology 10, 273-282.
- [6] JAHNKE E., EMDE F., 1945, *Tables of functions with formulae and curves*, Dover Publications.
- [7] LIVOLANT M., JEANPIERRE F., 1974, *Autoprotection des résonances dans les réacteurs nucléaires*, Rapport CEA-R-4533-1974.
- [8] MAO L., ZMIJAREVIC I., 2017, *A new Tone's method in APOLLO3[®] and its application to fast and thermal reactor calculations*, Nuclear Engineering and Technology 49, 1269-1286.
- [9] NUCLEAR ENERGY AGENCY, *Joint Evaluated Fission and Fusion (JEFF) Nuclear Data Library*, <http://www.oecd-nea.org/dbdata/jeff/>
- [10] PÁZSIT I., DEMAZIÈRE C., 2010, *Noise Techniques in Nuclear Systems*, In: Cacuci D.G. (eds) Handbook of Nuclear Engineering. Springer, Boston, MA.
- [11] RAVETTO P., 1997, *Reactivity oscillations in a point reactor*, Annals of Nuclear Energy 24, 303-314.
- [12] RIBON P., MAILLARD J. M., 1986, *Probability Tables and Gauss Quadrature: Application to Neutron Cross Sections in the Unresolved Energy Range*, NUREG/CP-0080-Vol1, United States.

- [13] ROUCHON A., 2016, *Analyse et développement d'outils numériques déterministes et stochastiques résolvant les équations du bruit neutronique et applications aux réacteurs thermiques et rapides*, PhD thesis, Université Paris-Saclay, France.
- [14] SANCHEZ R., CHETAINE A., 2000, *A Synthetic Acceleration for a Two-Dimensional Characteristic Method in Unstructured Meshes*, Nuclear Science and Engineering 136, 122-139.
- [15] SANCHEZ R., 2002, *Calcul des fuites*, Rapport DMT CEA, 149-171.
- [16] SANCHEZ R., 2015, *Some comments in neutron noise theory*, Annals of Nuclear Energy 86, 88-98.
- [17] SANTANDREA S., 2007, *An Integral Multidomain DP_N Operator as Acceleration Tool for the Method of Characteristics in Unstructured Meshes*, Nuclear Science and Engineering 155, 223-235.
- [18] SANTANDREA S., SCIANNANDRONE D., SANCHEZ R., MAO L., GRAZIANO L., 2016, *A Neutron Transport Characteristics Method for 3D Axially Extruded Geometries Coupled with a Fine Group Self-Shielding Environment*, Nuclear Science and Engineering 186, 239-276.
- [19] SCHNEIDER D., DOLCI F., GABRIEL F., PALAU J.-M., GUILLO M., POTHET B., ARCHIER P., AMMAR K., AUFFRET F., BARON R., BAUDRON A.-M., BELLIER P., BOURHRARA L., BUIRON L., COSTE-DELCLAUX M., DE SAINT JEAN C., DO J.-M., ESPINOSA B., JAMELOT E., JOUAULT V., LAUTARD J.-J., LENAIN R., LE PALLEC J.-C., MAO L., MASIELLO E., MENGELLE S., MOREAU F., MOSCA P., MUNIGLIA M., ODRY N., PASCAL V., PASTORIS S., ROQUE B., TARGA A., PATRICOT C., SANTANDREA S., SCIANNANDRONE D., TSILANIZARA A., VIDAL J.-F., ZMIJAREVIC I., 2016, *APOLLO[®] : CEA/DEN DETERMINISTIC MULTI-PURPOSE CODE FOR REACTOR PHYSICS ANALYSIS*, Conference paper, Physor at Sun Valley Idaho.
- [20] SCIANNANDRONE D., 2015, *Acceleration and higher order schemes of a characteristic solver for the solution of the neutron transport equation in 3D axial geometries*, PhD thesis, Université Paris Sud - Paris IX, France.
- [21] TELLIER H., 1993, *Cinetique des réacteurs nucléaires*, INSTN, CEA Collection enseignement.
- [22] Weinberg A. M., Schweinler H. C., 1948, *Theory of oscillation absorber in a chain reactor*, Physical review 74, 851-863.
- [23] YEE B. C., KOCHUNAS B., LARSEN E. W., XU Y., 2017, *Space-Dependent Wielandt Shifts for Multigroup Diffusion Eigenvalue Problems*, Nuclear Science and Engineering 188, 140-159.